T.C.
SAKARYA UNIVERSITY
INSTITUTE OF SCIENCE AND TECHNOLOGY

HIGH CAPACITY $LiFePO_4$/C/rGO NANOCOMPOSITE POSITIVE ELECTRODE FOR LITHIUM ION BATTERIES

M.Sc. THESIS

Ali Jamal Abdulkareem ABDULKAREEM

Department : NANOSCIENCE & NANOENGINEERING

Supervisor : Assoc. Prof. Dr. Tuğrul ÇETİNKAYA

January 2022

T.C.
SAKARYA UNIVERSITY
INSTITUTE OF SCIENCE AND TECHNOLOGY

HIGH CAPACITY $LiFePO_4$/C/rGO NANOCOMPOSITE POSITIVE ELECTRODE FOR LITHIUM ION BATTERIES

M.Sc. THESIS

Ali Jamal Abdulkareem ABDULKAREEM

Department : NANOSCIENCE & NANOENGINEERING

This thesis has been accepted unanimously / with a majority of votes by the examination committee on 10.01.2022

Head of Jury **Jury Member** **Jury Member**

DECLARATION

I declare that all the data in this thesis was obtained by myself under academic rules, all visual and written information was presented according to academic and ethical rules, there is no distortion in the presented data, any other persons' works were referred to according to scientific standards, and the data has not been used in any other thesis at the university or anywhere else.

Ali Jamal Abdulkareem

10.01.2022

ACKNOWLEDGEMENT

I would like to express my sincerest gratitude to my supervisor, Associate Professor.Tuğrul ÇETİNKAYA for his patience in helping me develop my thesis and guide my research.

I'd also like to express my gratitude to Res. Assist. Dr.Abdulkadir KIZILASLAN for his invaluable assistance. I'd like to express my gratitude to all of my laboratory friends for their unforgettably kind gestures and for all of the memorable moments I shared with them; in particular, I'd like to thank my friend Ahmed Faris, who was always there for me, ready to listen and support me under any circumstances.

Finally, I want to appreciate my parents. Their understanding and support have helped me to achieve my graduate degree.

TABLE OF CONTENTS

LIST OF SYMBOLS AND ABBREVIATIONS

A	: Ampere
Ar	: Argon
CV	: Cyclic voltammetry
°C	: Degrees Celsius
C	: Current , Carbon
cm	: Centimeter
EDS	: Energy dispersive X-ray spectroscopy
EIS	: Electrochemical impedance spectroscopy
FESEM	: Field emission scanning electron microscopy
F	: Faraday constant
SEM	: Scanning electron microscopy
Scm	: Standard cubic meter
LFP	: Lithium iron phosphate
Li+	: Lithium ions
LIP	: Lithium-ion battery
LFP/C	: Lithium iron phosphate and carbon nano composite
mAh	: MiliAmper.hour
μm	: Miceonmeter
NMP	: N-methyl pyrrolidone
PVDF	: Polyvinylidene fluoride
RAMAN	: Raman spectroscopy
rGO	: Reduce graphene oxide
R_E	: Electrolyte resistance
R_{CT}	: Charge transfer resistance
R_{SF}	: Surface film resistance
Scm	: Standard cubic meter

S	: Sucrose
SEM	: Scanning electron microscopy
T	: Temperature
Wt%	: Weight percent
XRD	: X-ray diffraction

LIST OF FIGURES

LIST OF TABLES

SUMMARY

Keywords: Li-ion, LFP, Carbon, Graphene, specific capacity, cycle life.

The development of new electrode materials with superior electrochemical capabilities, primarily dictated by the cathode materials, is required for widespread and extended applications of Li-ion secondary batteries. Because of its excellent stability, availability, and environmental friendliness, $LiFePO_4$ (LFP) is widely recognized as a viable cathode material. This study used a low-cost iron (III) as the base material to manufacture single-phase LFP material with submicron particles using a simple solution combustion process based on the glycine–nitrate technique. The optimal Glycine to $LiFePO_4$ ratio was found to be as 1:4 to produce high purity $LiFePO_4$ and produced $LiFePO_4$ showed 102 mAh/g discharge capacity at the constant rate of C/20.

Sucrose was utilized as a carbon source to obtain carbon-coated $LiFePO_4$ powders. The discharge capacity of the as-prepared $LiFePO_4$/C sample with 12% carbon content is around 157 mAh/g at a 0.1 C rate and 88 mAh/g at a 5 C rate. Furthermore, throughout the 50-cycle at varying current rates, the electrodes showed excellent cycling performance.

To enhance the capacity of carbon-coated $LiFePO_4$, different amount of Graphene was reinforced to the cathode material. The carbon-coated lithium iron phosphate with 4 wt.% graphene showed a specific capacity of 197 mAh/g. The highly conductive graphene flakes wrapped around carbon-coated lithium iron phosphate enhance electron migration during charge and discharge operations, decreasing irreversible capacity during the first cycle and resulting in a coulombic efficiency of 99% at varied C-rates.

LİTYUM İYON PİLLER İÇİN YÜKSEK KAPASİTE $LiFePO_4$/C/rGO NANOKOMPOZİT POZİTİF ELEKTROT

ÖZET

Anahtar kelimeler: Li-İyon Pil, LFP, Karbon, Grafen, Spesifik Kapasite, Çevrim Ömrü

Li-ion ikincil pillerin yaygın ve genişletilmiş uygulamaları için, öncelikle katot malzemeleri tarafından belirlenen üstün elektrokimyasal yeteneklere sahip yeni elektrot malzemelerinin geliştirilmesi gereklidir. Mükemmel stabilitesi, kullanılabilirliği ve çevre dostu olması nedeniyle, $LiFePO_4$ (LFP), uygulanabilir bir katot malzemesi olarak yaygın olarak kabul edilmektedir. Bu çalışmada, glisin-nitrat tekniğine dayalı basit bir çözelti yakma işlemi kullanılarak mikron altı parçacıklara sahip tek fazlı LFP malzemesi üretmek için temel malzeme olarak düşük maliyetli bir demir (III) kullanılmıştır. Yüksek saflıkta $LiFePO_4$ üretmek için optimal Glisin/$LiFePO_4$ oranı 1:4 olarak bulunmuş ve üretilen $LiFePO_4$, sabit C/20 oranında 102 mAh/g deşarj kapasitesi gösterdi.

Karbon kaplı $LiFePO_4$ tozları elde etmek için karbon kaynağı olarak sakroz kullanılmıştır. %12 karbon içerikli $LiFePO_4$/C numunesinin deşarj kapasitesi 0,1 C akım hızında 157 mAh/g ve 5 C hızında 88 mAh/g olarak elde edilmiştir. Ayrıca, 50 döngü boyunca değişen akım hızlarında elektrotlar mükemmel döngü performansı göstermiştir.

Karbon kaplı $LiFePO_4$'ün kapasitesini arttırmak için katot malzemesine farklı miktarlarda grafen ile takviye edilmiştir. Ağırlıkça %4 grafenli karbon kaplanmış lityum demir fosfat, 197 mAh/g'lik bir spesifik kapasite göstermiştir. Karbon kaplı lityum demir fosfatın etrafına sarılmış son derece iletken grafen pulları, şarj ve deşarj işlemleri sırasında elektron göçünü hızlandırmış ve ilk döngü sırasında tersinmez kapasiteyi azaltmış ve farklı C-hızlarında %99'luk bir kulombik verim sergilemiştir.

CHAPTER 1. INTRODUCTION

In recent years, due to various factors including global warming, pollution challenges, and the increase of fossil fuels, attention has been redirected to finding an alternative source to fossil fuels or reducing their usage. One of these considerations is the use of electricity from battery energy, which is considered both an efficient and safe method in the long-term reflection of reducing fossil fuels, leading to a decrease in emissions of greenhouse gases and air pollution. Despite the fact that battery development has played an important role in the development of portable gadgets and mobile technologies, even though technology has been around for over a century, it cannot still offer the performance necessary for huge devices. The inability is due to the lack of providing these services at a competitive cost, due to their requirements of a high energy density, a compact size, a low price, and quick charging rates as well as the ability to store and run at a high current. However, the usage of batteries in large appliances continues to increase (Larry Feinberg, 2016).

Primary and secondary batteries are the two types of batteries available, with both of them considering the battery to be a powerful device that provides electricity from chemical energy. Primary batteries contain material that cannot be returned to their original form after reaction occurs (due to chemical reasons being hard to reverse), because of this, it makes them generally non-chargeable and disposable. This is different from secondary batteries, which can be recharged many times over. This occurs as the chemical reactions can be reversed after each discharge using an electric current during discharging, allowing the reusability of the battery. Because of its optimal volumetric and gravimetric power output, the lithium-ion battery presented in this study is regarded as the best among the other varieties. (M.S. Whittingham, 2004). Different electrochemical performances of LIBs compared to other rechargeable batteries can be exhibited in Table 1.1. Firstly, there is practically no memory effect for LIB, hence, they allowed for charge ability at any time. It can also be seen that

LIBs have an energy density and a cell voltage that are double of that other types of rechargeable batteries. Furthermore, while they are at a significantly higher cost, LIBs feature low self-charge, long-life cycle, stability, and wide operating temperatures betwwen -20 °C and +60 °C. Taking all these factors into account, LIB utilizations can provide a safer and more efficient transportation system, due to its ability to act as a reliable rechargeable system. However, LIBs, due to of low charge/discharge rate, still act as a limitation in the application of high power tools and devices, including electric cars and bikes. In 1991 SONY company first commercially produced LIBs, from then they have been the most popular rechargeable batteries for portable and low energy devices, including laptop computers, cell phones, and cameras.

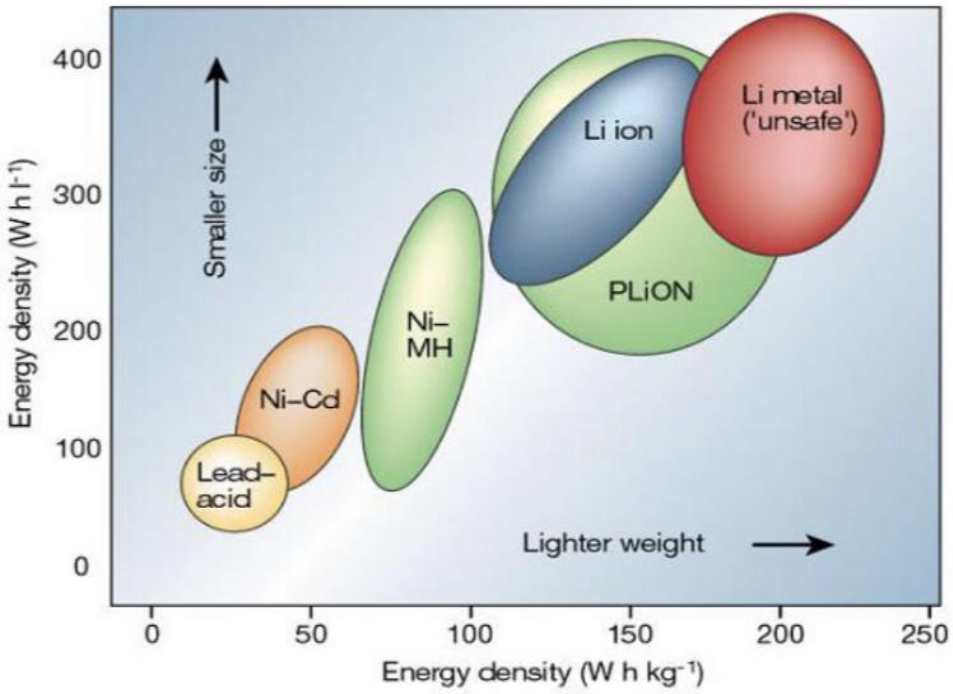

Figure 1.1. Comparing the volumetric and gravimetric power densities of various rechargeable batteries (Larry Feinberg, 2016).

As a consequence, LIB will find it challenging to meet the operational needs of the large appliances in the future, such as electric cars (EVs) or hybrid vehicles (HEV). As a consequence, further research is needed to improve the performance of the frequently used LIB to achieve an excellent performance battery, especially in terms of power/energy density, life cycle, and safety concerns.

The anode, cathode, and electrolyte components all have an impact on LIB's performance. Nonetheless, the cathode material, which has a lower specific capacitance than the graphite anode material, is presently the most important factor in LIB energy density (Larry Feinberg, 2016). In the LIB system, the primary step for rate determination is Li transfer/diffusion on the cathode (M.S. Whittingham, 2004). $LiCoO_2$ is a popular cathode material in LIB applications. However, because of CO, it is exceedingly costly and undesirable for the environment (‘Electrochimica Acta’, 2004). Because of its inexpensive cost, great thermal stability, abundance in nature, and environmental friendliness, $LiFePO_4$ is the best cathode material among the option (Padhi, Nanjundaswamy and Goodenough, 1997).

However, it has some disadvantages, such as low electrical conductivity, low charge/discharge current densities, and ion diffusion is low, which restricts its use in large types of devices. (Padhi, Nanjundaswamy and Goodenough, 1997).

Table 1.1. Variations in rechargeable battery performance characteristics (Ravet *et al.*, 2001).

Types of battery	Energy density (Wh/kg)	Cycle durability	Self-discharge (peer month)	Cell voltage (V)	Charge time (h)
NiMH	30-80	500-1000	25%-30%	1.2	2-4
NICD	40-60	1500	10%-20%	1.25	1
Lead-acid	30-40	600-800	5%-20%	2.1	8-16
Li-ion	100-170	1200	5%_12%	3.5	1-3

Reduced particle sizes and coatings with high conductivity materials, such as carbon(Yamada, Chung and Hinokuma, 2001; Herle *et al.*, 2004), have been used to try to solve these problems. As a result, it is expected that by optimizing particle size, morphology, and carbon coating, the performance of these materials will be improved at higher current rates.

Differences in crystallinity, particle sizes, purity, morphology, and electrochemical performance of $LiFePO_4$ depend on the procedures and conditions of the preparation (Ferrari *et al.*, 2010; Gong and Yang, 2011). Certainly, obtaining high-performance materials will require a successful installation and optimal preparation. Since $LiFePO_4$

was introduced by Padhi et al. in 1997 (Padhi, Nanjundaswamy and Goodenough, 1997), several methods have been proposed to prepare $LiFePO_4$. including solid state, sol-gel, hydrothermal, co-precipitation, polyol process, microwave processes, etc (Jugović and Uskoković, 2009; Gong and Yang, 2011). The solid state synthesis is the most widely used technology owing to its simple approach and simplicity of scaling. (Arumugam, Paruthimal Kalaignan and Manisankar, 2009; Song *et al.*, 2010). However, this method has several disadvantages, such as high temperature sintering processes for long periods and high energy consumption. In addition, this method suffers from uncontrollable particle growth and agglomeration.

The hydrothermal synthesis yields $LiFePO_4$ materials with well-controlled shapes and small crystal particles in a fast, low-cost, scalable, and low-energy method. (Ellis *et al.*, 2007; Ou *et al.*, 2008; Zhang, 2010). Sol-gel, as another important method, ensures small particle size and higher purity, homogeneity due to optimum mixture of precursors (Chernova *et al.*, 2009; G. Wang *et al.*, 2010; Devaraju and Honma, 2012). Additionally, $LiFePO_4$ can be prepared simply and economically. As a result, sol-gel and hydrothermal processes are two of the most effective ways to make high-quality $LiFePO_4$ materials.

CHAPTER 2. LITHIUM ION BATTERIES

2.1. The Principle of Lithium Ion Batteries

Lithium ion rechargeable battery electrodes are made up of lithium intercalation compounds that reversibly accommodate lithium ions into their crystal structure. Unlike conversion electrode reactions, these can maintain their crystal structure during charge and discharge processes. Because the structure is stable throughout the charging and discharging operations, this mechanism allows for high power and cycle capability. On the other hand, intercalation compounds have a restricted capacity of roughly 250 mAh/g, which corresponds to a one-electron redox potential (Whittingham, 2008). In contrast to the intercalation process, conversion reaction molecules have a larger energy storage capacity. Figure 2.1. depicts a schematic depiction of these systems. In traditional lithium ion batteries, the cathode and anode often have a layer or tunnel structure.

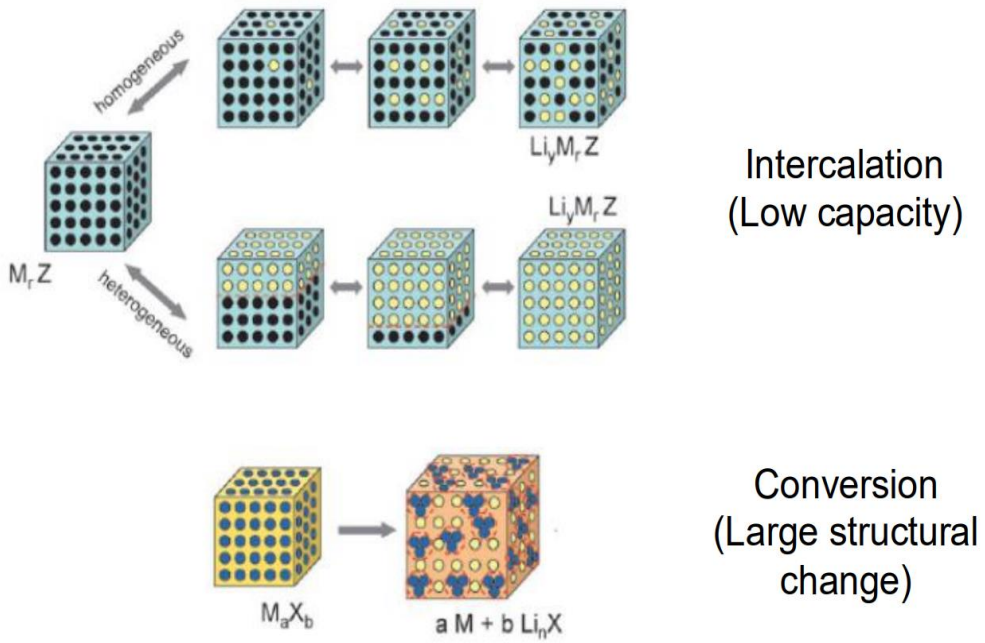

Figure 2.1. Electrochemical energy storage: intercalation and conversion reactions (Palacín, 2009).

A common lithium cell architecture is depicted in Figure 2.2. There are three pieces to a battery. They are the anode (positive electrode), the cathode (negative electrode), and the electrolyte (electrolyte). The differential in lithium atom concentration in the cathode and anode is the process by which lithium-ion batteries function. When the battery is charged, Li^+ flows from the anode to the negative electrode. Li^+ will return to the anode after the battery is drained. An electrochemical oxidation reaction occurs in the anode materials during the discharge operation. Li-ions are freed into the electrolyte during the electrochemical oxidation reaction. The cathode will gather Li-ions as they travel through the electrolyte. At the same time, electrons are traveling across the outside circuit and towards the negative electrode. The discharge period is the inverse of the charging period.

The cell potential is determined by the difference between the anodic and cathodic chemical potentials of lithium in these two host substances. A lithium ion cell's open circuit or theoretical standard potential is characterized as a rocking chair movement in which the chemical potential of Li ions (Equation-2.1) varies at each state between anodes and cathodes.

$$E_0 = -(\mu Li/+ - \mu Li/-)/nF \quad (2.1)$$

Here, E_0 represents equilibrium cell potential, $\mu_{Li/+}$ and $\mu_{Li/-}$ represent the chemical potentials of lithium in positive and negative electrodes, respectively; n represents the number of electrons involved in the reaction, and F is Faraday's constant.

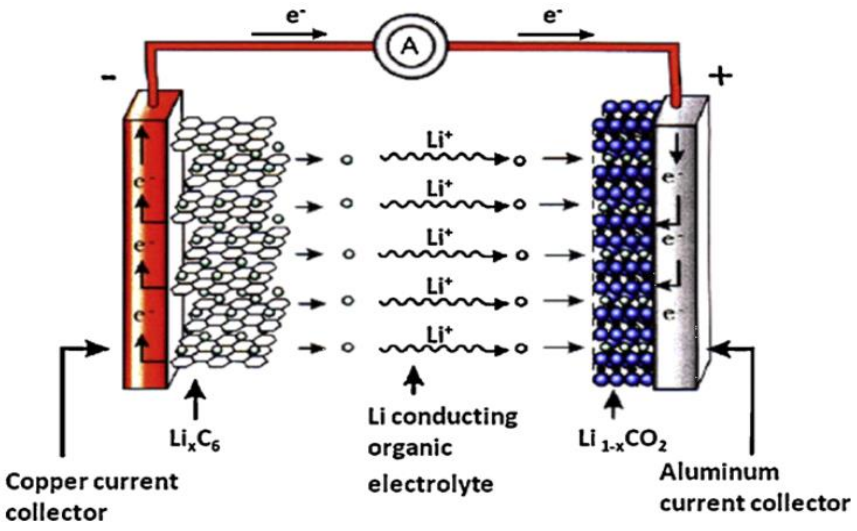

Figure 2.2. A rechargeable lithium ion battery's charging and discharging processes (Oh *et al.*, 2010).

The electrolyte in a high-power cell must sustain a high current on produced species throughout each cycle while avoiding irreversible processes and side products such as the solid electrolyte interface (SEI). If the galvanic cell potential goes below open-circuit voltage, battery power and cycle time are reduced. For a high-power cell, certain kinetic requirements of an electrode material are as follows:

1. In comparison to the Li/Li^+ couple, there is a large electrochemical potential gap between the positive and negative electrodes.
2. Lithium diffusivity in solids is high.
3. Lithium intercalation capacity is high.
4. Stable to electrochemical cycling.
5. Simple lithium intercalation kinetics.
6. Conductive to electricity.

2.2. Materials for the Lithium Ion Batteries

The anode, cathode, and electrolyte elements all play a significant role in LIB's performance (Armand and Tarascon, 2008; Larry Feinberg, 2016). Therefore, many research efforts have been undertaken to improve new materials for components of LIBs, Specifically, anode and cathode active compounds. The following are the primary characteristics of premium active substances:

1. Big quantity of Li^+ ions for intercalation/de-intercalation to increase the capacity.
2. Intercalation/de-intercalation of electrons and Li^+ ions is efficient and quick.
3. During the Li^+ ions intercalation/de-intercalation process the reversibility is good with a little or no change in host structure.
4. It retains chemical stability in the presence of an electrolyte without interacting with it.
5. Excellent electrical conductor to heat generation and reduce polarization.
6. Environmental friendly, inexpensive, lightweight, simple to synthesize.

when the LIB was introduced two decades ago. Most studies focused on cathode materials to progress the performance of LIBs due to the intercalation capacity of cathode material is substantially lower, especially when it is compared with anode materials in long-term cycles (M.S. Whittingham, 2004). Additionally, other aspects of a positive cathode material include materials prices, safety concerns, recyclability, and environmental toxicity. As a result, the cathode material is the focus of lithium-ion battery electrode research.

2.2.1. Anode materials

Lithium metal was utilized as the anode in the first LIB since it is the lightest metal with the lowest voltage (-3.045V) as well as a high capacity (3826 mAh g^{-1}). Which can easily release the electron. Nevertheless, because of the short circuits caused by the growth of lithium dendrites on the surface of the lithium metal anode during cycling, the use of lithium metal as an anode poses a significant risk in lithium batteries (Balakrishnan, Ramesh and Prem Kumar, 2006). It's also extremely reactive to oxygen and moisture. As a result, dry rooms or glove boxes are required for the LIB to be assembled. Furthermore, while the Li-Al alloy eased the safety issue, it was still unable to prevent fast capacity decline (Rao, Francis and Christopher, 1977).

After sundry researches, graphite with a specific capacity of 379 mAh/g was presented as the anode material that could host Li^+ ions during interaction with the metering of

the elements in LiC_6 (Yazami and Touzain, 1983). Sony commercialized graphite as an anode for LIBs in 1991 (] Nagaura .T, 1990). using graphite instead of lithium metal not only solves the safety problem but also minimizes the cost (Ferg *et al.*, 1994; Winter and Besenhard, 1999).

The elements used in lithium-ion batteries are depicted in Figure 2.3. (Nitta and Yushin, 2014). Tin (Sn), tin oxide (SnO_x), silicon (Si) and silicon dioxide (SiO_x) are some of the anode materials that have gotten a lot of interest from researchers. The Si anode material has shown favorable characteristics among these anode materials.

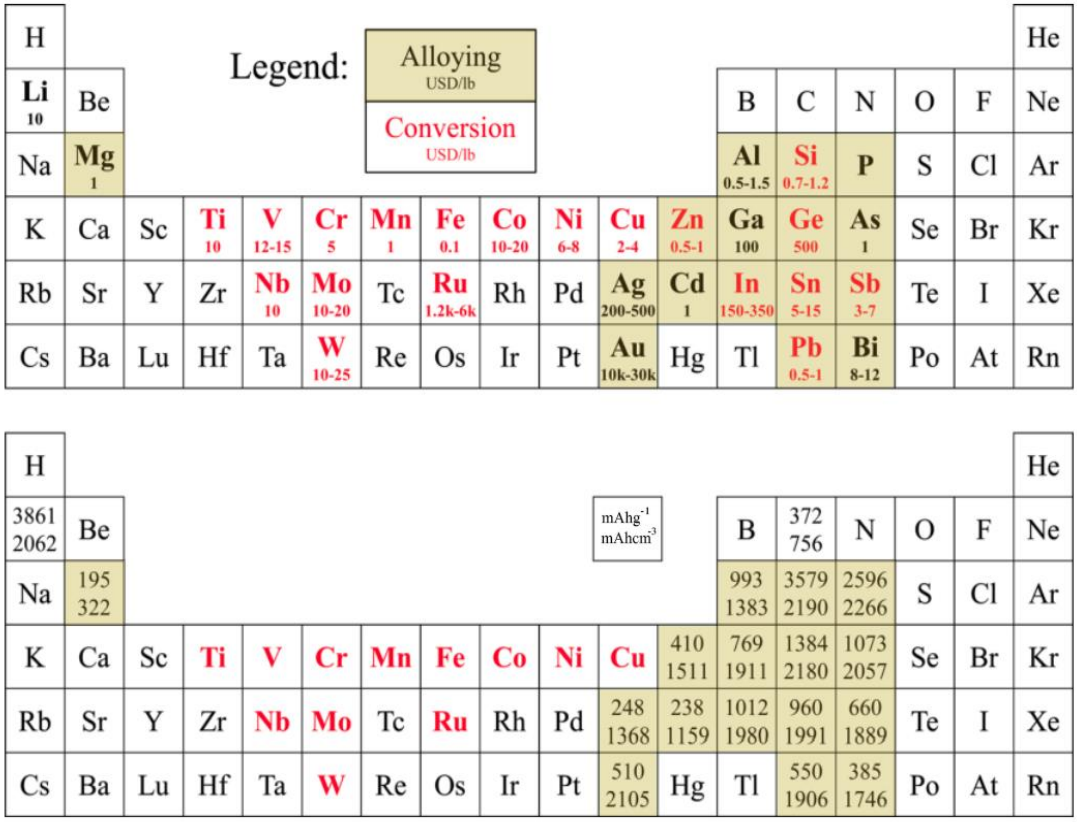

Figure 2.3. Li-ion battery anode materials investigated for high capacity (Nitta and Yushin, 2014).

Batteries require both anode and cathode materials to function properly. There has been a lot of work done to improve the anode and cathode characteristics. Power density, energy density, and cycle life are all factors in anode material performance. When used as an anode material, it has the maximum energy density when the voltage is low.

2.2.2. Cathode materials

The cathode materials in lithium ion batteries have drawn a lot of attention from researchers since they have a big impact on the batteries (Larry Feinberg, 2016). As a cathode for LIB applications, a premium material must meet the following requirements (M.S. Whittingham, 2004):

1. In order to get a high voltage output from the battery, the metal ion should have a high redox potential.
2. In order to get high battery capacity, the structure should allow a large number of lithium ions reversible interaction and extraction.
3. To give appropriate capacity, host high lithium ions.
4. High surface area to raise the rates of reduction/redox reaction.
5. The electronic conductivity should be high to rapidly transfer the electron and reduce heat generation.
6. High ionic conductivity to assure high capacity and minimal polarization.
7. The material structure must maintain stability during repeatedly charging and discharging operations to ensure a good cycle ability.
8. Abundant, low cost, environment friendly, and easy to prepare.

As illustrated in the diagram below (Figure 2.4.), intercalation cathode materials for LIBs are classified into three categories based on their crystal lattice: layered, spinel, and olivine (Thackeray, 2002):

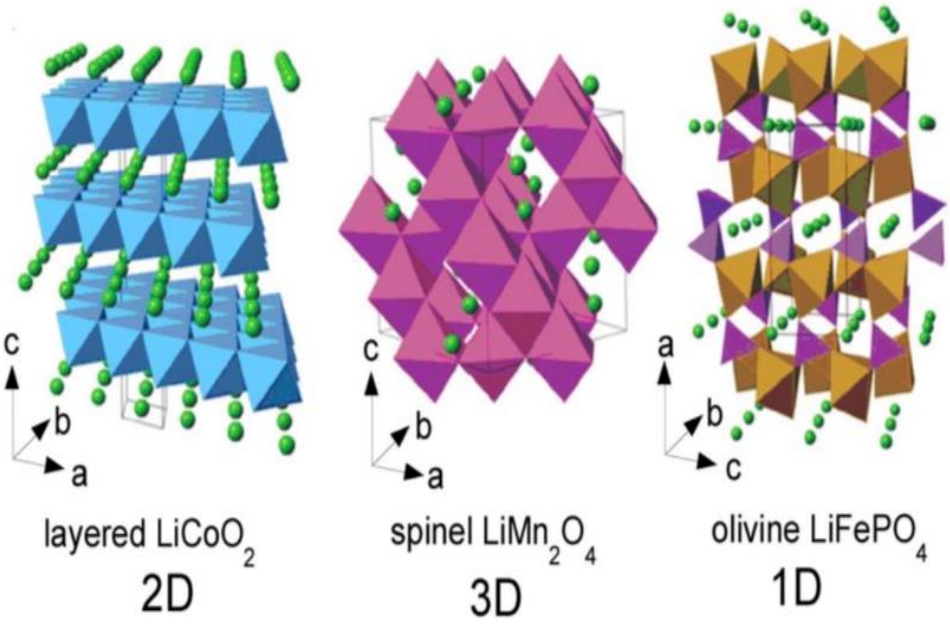

Figure 2.4. Models for Li^+ transport in layered, spinel, and olivine structures (Thackeray, 2002).

Table 2.1. lists the cathode materials for each of the three frameworks. The transition metal oxide is currently the focus of the majority of cathode material research. Since the invention of lithium-ion batteries in 1990, $LiCoO_2$ has been the first transition metal oxide material. It has a layered structure. $LiCoO_2$ has a high theoretical specific capacity of 274 $mAhg^{-1}$, 1363 $mAhg^{-1}$ theoretical volumetric capacity, low self-discharge, high discharge voltage, and strong cycle performance (Du Pasquier *et al.*, 2003).

Table 2.1. Cathode materials classified by different framework (Julien *et al.*, 2014).

Framework	Compound
layered	$LiCoO_2$
	$LiNi1/3Mn1/3Co1/3O_2$
spinel	$LiMnO_4$
	$LiMn3/2Ni1/2O_4$
olivine	$LiFePO_4$
	LiFe1/2Mn1/2PO4

Table 2.2. The comparison between different cathode materials (Julien *et al.*, 2014).

Cathode	$LiCoO_2$	$LiMnO_4$	$LiNiO_2$	$LiFePO_4$
Capacity/$mAhg^{-1}$	274	148	274	169
Potential/V	3.90	4.05	3.60	3.40
Density/g cm^{-3}	5.10	4.31	4.85	3.60

However, these cathode materials have limitations in terms of cost, thermal stability, and capacity decline at high current rates (Nitta *et al.*, 2015). Because of the Mn, the spinel $LiMnO_4$ has a cheap cost and is environmentally friendly. However, the capacity and other characteristics are are comparable to $LiCoO_2$. Polyanions have been developed as a result of a recent study into cathode materials. SO_4, PO_4, and SiO_4 are examples of polyanions. They take up lattice sites and raise the redox potential of the cathode. The olivine structure $LiFePO_4$ belongs to the polyanions (Nanjundaswamy *et al.*, 1996).

2.2.3. Binder for the lithium battery

In lithium ion batteries, the binders have a significant important on the performance of the electrode. The active anode particles are mixed with conductive carbon particles and a binder to make a battery cell (3-15 %). Polyvinylidene fluoride (PVDF), a thermoplastic polymer with poor elastomeric properties, is the typical binder for graphite and metal anodes. As a result, it's reasonable to think that an alternate elastomer binder, such than PVDF, might be better at supporting significant volume changes in alloy particles (Chen *et al.*, 2004). Using cross-linking polymers and an elastomer binder system, this notion has been shown to improve the cycling stability of various alloy anodes (Liu *et al.*, 2005). The premise was challenged when it was discovered that a stiff, brittle sodium carboxymethyl cellulose (CMC) binder was even more effective than PVDF or a styrene-butadiene rubber (SBR) elastomer binder in boosting the capacity retention of Si anode (Chen, Christensen and Dahn, 2003). This finding indicates that other parameters play a significant role in addition to elastic elongation. The CMC binder may operate as a surface modification, helping to establish a stable SEI passive layer.The expanded structure of CMC in solution, according to Lestriez et al (Lestriez *et al.*, 2007), resulted in a more homogenous

dispersion and networking of the conductive carbon and active particles. Winter et al (Hochgatterer *et al.,* 2008). claimed that the improved reversibility of Si/C electrodes made with CMC binder was due to the establishment of a strong chemical link between the binder and the active particles (Si). They claim that the cohesive strength of the binder and active particles are crucial components. In a recent paper, it is reported that a lithium polyacrylate (Li-PAA) binder performed even better than CMC binder (Chen *et al.,* 2006). Capacity retention was good at 450 mAh/g when employing a Li-PAA binder on an amorphous SnCoC electrode for at least 100 cycles, compared to fewer than 20 cycles when using PVDF or CMC binders. These findings indicated that the binder system used has a significant influence on the performance of active materials. More research is needed to properly understand the beneficial effects of diverse binder systems.

2.2.4. Electrolyte for lithium batteries

The electrolyte composition, in addition to the binder, has a considerable influence on the cycle stability of lithium batteries (Zhao *et al.*, 2008). The most extensively utilized electrolyte for lithium-ion batteries is LIPF6 dissolved in carbonates, such as ethylene carbonate (EC), dimethyl carbonate (DMC), and diethyl carbonate (DEC). This electrolyte performs admirably under normal conditions, but its low temperature performance will be limited below -20°C. Lithium batteries' poor performance at low temperatures is due not only to the high viscosity and low transference of Li-ions in the electrolyte but also from the high de-solvation energy of the Li^+. The electrolyte composition has a significant impact on lithium-ion battery cycling stability. Furthermore, the electrolyte is crucial for lithium battery safety. The following are some of the issues with current $LIFP_6$ organic carbonate solution electrolytes:

1. There is a relatively narrow range of cathode stability, so high voltage cathodes are not acceptable.
2. The high vapour pressure and the flammability have a negative impact on safety and health, and result in serious manipulation risks.

A lot of work is being done to improve the safety and dependability of Li-ion battery electrolytes, including:

1. Additives to create a stable SEI and/or improve it's thermal stability.
2. Redox shuttles provide overcharge protection.
3. Separators are turned off to prevent thermal runaway.
4. Lithium salts as a low-toxicity alternative to $LIPF_6$.

2.2.5. Separators

The separator in a lithium-ion battery prevents a short circuit in the battery by preventing electron passage between the cathode and the anode, while also allowing lithium ions to flow between the cathode and the anode in the electrochemical cell. The separator in lithium-ion batteries allows ions to travel through while preventing contact between the anode and the cathode. placed between the positive and negative electrodes. The separator must be thermally, chemically, and electrochemically stable to the electrolyte, have a micrometer-sized porous structure, and be mechanically durable to tolerate high currents.

Polypropylene (PP) and polyethylene (PE) films are commonly used in commercial lithium-ion batteries. The reason why polypropylene and polyethylene are preferred is that they allow the battery to work without deterioration even in long cycles in lithium ion batteries and are protected inside the battery without deterioration. However, polypropylene may not have the width to prevent a short circuit and may cause a short circuit. This ensures that the battery does not work. Therefore, polyethylene is used more in lithium-ion batteries than polypropylene.

CHAPTER 3. $LiFePO_4$ BASED CATHODE

3.1. $LiFePO_4$ Electrode

Lithium iron phosphate ($LiFePO_4$) is a promising alternative to lithium cobalt oxide as the cathode in lithium-ion batteries attributed to its inexpensive cost, abundance in nature, great thermal stability, nontoxicity, and long cycle life (Padhi and Goodenough, 1997; Liu *et al.*, 2009). Preparing $LiFePO_4$ can involve several methods, including but not limited to the sol-gel method (Hu *et al.*, 2004), the hydrothermal method (Kim *et al.*, 2008; Song *et al.*, 2011), co-precipitation (Yang, Zavalij and Whittingham, 2001), microwave processes (Ding *et al.*, 2010), the solid-state method (Liu *et al.*, 2006). The low electrical conductivity of pristine $LiFePO_4$ and its poor ability to diffuse ions make it unsuitable for large applications due to its poor diffusion properties ($10^{-14}cm^2s^{-1}$) (Huang, Yin and Nazar, 2001). To counteract this, particle size reduction, carbon coating, and metal doping are among the several strategies proposed (Wang and Cao, 2008; Cheng *et al.*, 2010). From these, carbon coating has the most support regarding its further study compared to the other methods, such as doping and particle sizes reduction, due to a more significant impact on performance from experimental results (Belharouak, Johnson and Amine, 2005; Zhang *et al.*, 2008).

The problem with poor electrical conductivity might be fixed by using conductive porous films of carbon to apply a coating on the surface of particles (Cheng *et al.*, 2010). Furthermore, By covering the electrode material with carbon, the material is prevented from dissolving in the electrolyte and the electrolyte from seeping into it, so resolving the issue of direct interaction between the electrode and the electrolyte (Noh *et al.*, 2005). When carbon coating is applied, undesirable particle formation during the production of $LiFePO_4$ is also inhibited. This is because it will function as a reducing agent, preventing the oxidation of Fe^{2+} to Fe^{3+}. (Chen *et al.*, 2008; Zaghib *et al.*, 2008).

Various sources of carbon can be used in this application and are considered suitable, including ascorbic acid (Yang *et al.*, 2011), lactose (Liang *et al.*, 2008), sucrose (Wang, Shen and Yao, 2009), glucose (Zhou *et al.*, 2011), carbon nanotube (Saravanan *et al.*, 2010), graphene (Su *et al.*, 2010), however, the source must be inexpensive. Moreover, in order to assure $LiFePO_4$ particles have excellent conducting properties, two features need to be considered, the first being a uniform carbon coating while the second being an optimized amount (Spong, Vitins and Owen, 2006; Doeff *et al.*, 2008). The latter point is of importance, as if large amounts of carbon are used, a significant number of side effects can occur as a result, for instance, the reduction of $LiFePO_4$ to Fe_2P, porosity decreases, as does energy density (Dominko *et al.*, 2005; Kang *et al.*, 2012). The former regarding the uniform application, of the homogenous carbon coating on the surface of $LiFePO_4$ particle is currently a challenging process, specifically, no current literature fulfills the conditions for lithium-ion batteries (L. Wang *et al.*, 2010). To maximize the performance of the electrode based on these electrodes, the amount of carbon utilized for the coating, the uniformity of the coating, and the physicochemical parameters of the coating should be considered. This shows, therefore, that the objective is to enhance the carbon quantity, in order to obtain a homogenous covering while retaining its energy density. To examine the effect of carbon on the structure, morphology, performance, and electrochemical properties of $LiFePO_4$, $LiFePO_4$ with varying concentrations of sucrose as a carbon source is produced.

3.2. Structure of $LiFePO_4$

$LiFePO_4$ has an orthorhombic olivine structure (Padhi *et al.*, 1997). Figure 3.1. depicts its crystal structure. The unit cell volume of $LiFePO_4$ is $0.291392nm^3$, and the lattice parameters are a=0.6008nm, b=1.0334nm, and c=0.4693nm. The oxygen atoms in $LiFePO_4$ are placed in a somewhat deformed hexagonal close packing fashion, P atoms occupy tetrahedral positions to create the PO_4 tetrahedron, and Li and Fe atoms fill the oxygen octahedral gap (Andersson and Thomas, 2001). Li atoms occupy common edge octahedral M1 (100) sites while Fe atoms occupy common angle octahedral M2 (010) sites, respectively, to produce the LiO_6 octahedron and the FeO_6 octahedron. The

layered scaffold structure is made up of LiO_6 octahedrons, FeO_6 octahedrons, and PO_4 tetrahedrons that are alternately organized. On the bc plane, adjacent FeO_6 octahedrons produce FeO_6 layers by sharing oxygen atoms as common vertexes. An adjacent LiO_6 octahedrons use two oxygen atoms along the same edge to build a chain in the b direction among the FeO_6 layers. Two oxygen atoms are shared along the border of one PO_4 tetrahedron and one FeO_6 octahedron.

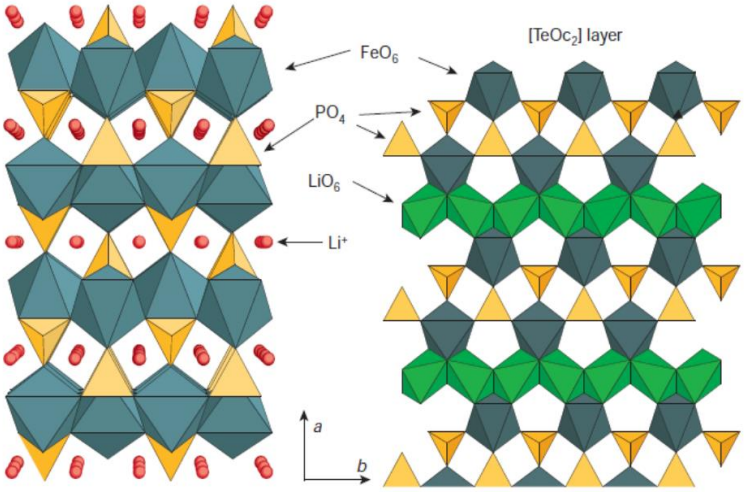

Figure 3.1. Schematic of the crystal structure of $LiFePO_4$ (Padhi *et al.*, 1997).

3.3. Intrinsic Problems of the Olivine Structure

In $LiFePO_4$, the FeO_6 octahedrons share the same vertices, but they are separated by the PO_4 tetrahedrons. As a result, the FeO_6 octahedrons are unable to create a continuous octahedron network since their structures share the same edges. The electronic conductivity of the material will be drastically reduced as a result of this feature (Wang, He and Zhou, 2011). It is an intrinsic n-type semiconductor by definition. However, due to the huge band gap of 3.7eV calculated by the First Principle (Andersson *et al.*, 2000), intrinsic $LiFePO_4$ has a relatively low electrical conductivity at ambient temperature, resulting in weak electrochemical performance when subjected to high current loads. Meanwhile, due to the hexagonal close packing order of the oxygen atoms, they can only supply a limited number of pathways for Li^+ ions. As a result, at room temperature, the rate of Li^+ ion migration is relatively low (Yamada *et al.*, 2003; Morgan, Van der Ven and Ceder, 2004).

Padhi (Padhi *et al.*, 1997) was the first to report the use of $LiFePO_4$ for potential application in Li-ion batteries. At ambient temperature and low current density, there were only 0.6mol Li^+ ions (equal to 110mAh/g) participating in the intercalation/extraction reaction per mole of $LiFePO_4$ (Tarascon and Armand, 2001). The $LiFePO_4$ charge-discharge method, according to Padhi, is a Li^+ ion diffusion control process. When the current density is increased, the specific capacity drops dramatically; if the current density is reduced further, the specific capacity returns to its former value. Takahashi et al. (Takahashi *et al.*, 2002) later investigated the effect of current density on discharge capacity at various temperatures. With an increase in current density at 20°C, the discharge capacity dropped. Along with the increase in temperature, the discharge capacity increased as well. The rate of diffusion increases with an increase in operating temperature. The Li^+ ion diffusion control theory is backed up by this study.

3.4. The Mechanism of Li^+ Extraction and Insertion in $LiFePO_4$

The primary functioning concept of $LiFePO_4$ is the Li^+ diffusion process. This diffusion process comprises the insertion/extraction of lithium. Understanding this process is essential for comprehending the $LiFePO_4$ cathode technique. During charging, Li^+ exits from $LiFePO_4$ and moves towards the anode electrode. Two phases can be observed in this charge/discharge process. Both $LiFePO_4$ and $FePO_4$ phases can exist simultaneously. Li_xFePO_4 is generally described as this two-phase reaction (Takahashi *et al.*, 2001). A unique model was proposed by Laffont (Laffont *et al.*, 2006) to clarify the $LiFePO_4/FePO_4$ phase change process. During the charge/discharge process, it resembles the fundamental structural models. When the battery is charging, lithium ions are extracted from the particles' centers at first. Li^+ will begin to be injected from the outer layer during the discharge process. This implies that $LiFePO_4/FePO_4$ always has a fundamental structure. Another suggestion from Delmas (Delmas *et al.*, 2008) to describe the process of transformation is the domino-cascade. In accordance with his model, when Li^+ begins to be inserted/extracted into a single particle, the particle will become fully charged or discharged. As a result,

utilizing X-ray microscopy to monitor the change between the $LiFePO_4$ and $FePO_4$ phases throughout the charge/discharge process is an essential step. The charge and discharge reactions are as follows (Takahashi *et al.*, 2001):

- Charge reaction: $LiFePO_4 - xLi^+ - xe^- \Rightarrow xFePO_4 + (1-x)LiFePO_4$
- Discharge reaction: $FePO_4 + xLi^+ + xe^- \Rightarrow xLiFePO_4 + (1-x)FePO_4$

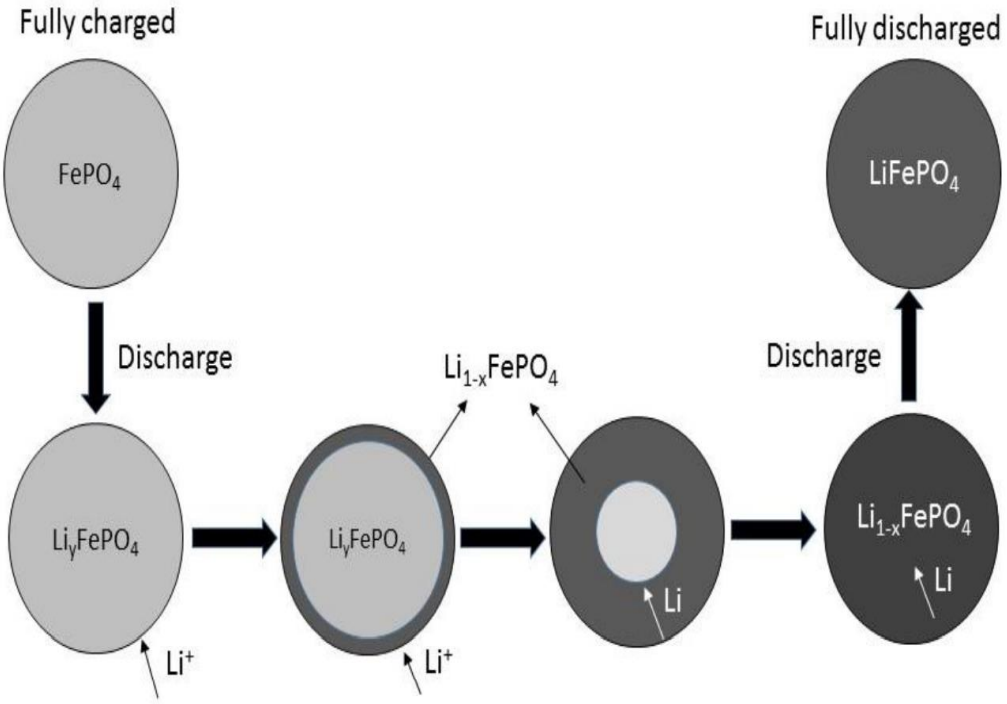

Figure 3.2. Li^+ insertion process (discharge process).

3.5. The Challenges of $LiFePO_4$

$LiFePO_4$ is still having some problems as the cathode material. It has low tap density. It also performs poorly at low temperatures. The bulk density of a material is expressed as the quantity of numerous particles split by the entire volume of the particles. From table two, $LiFePO_4$ has the lower theoretical density as compared with the other cathode materials. It's only 3.60 gcm^{-3}. Most $LiFePO_4$ has a density of only 1 to 1.4 g cm^3 (Yuan *et al.*, 2011). For materials as a powder, both particle morphology and theoretical density can determine the bulk density. The particle morphology comprises both particle distribution, particles size, and geometric shapes. Like the higher carbon

content will reduce the density, and smaller particle size will also reduce the density (Yuan *et al.*, 2011). For $LiFePO_4$ cathode materials, both carbon coating and small particle size are important for modifier performance, so this results in a paradoxical issue that causes low LFP density. Lower tap density will result in limited LFP use in a handheld device. Another disappointing performance is the LFP's bad performance at low-temperature. As the report of the 45th Battery Symposium in Japan proved (Yuan *et al.*, 2011), Lowering the temperatures result in lower capacity for LFP batteries. This flaw prevents the battery from meeting the standards for electric cars. The LFP battery's electrolyte suffers from the same issue. The Li^+ diffusion between the electrode and the electrolyte is limited as the temperature decreases, especially under -20°C.

3.6. Improvement of $LiFePO_4$

As mentioned earlier, $LiFePO_4$ is beneficial in aspects of safety, non-toxicity, environmental friendly, low cost, high quality ability, good life cycle, etc. But it has limited lithium ion diffusion rate and poor electrical conductivity, and this is not suitable for high current discharge/charge. The shape, crystalline size, and carbon coating are three aspects that might be modified to increase the performance of LFP batteries. As the particle size decreases, Li^+ will have a larger electrolyte/electrode contact area and shorter diffusion lengths. Spherical shapes can have higher bulk density when compared with irregular shapes. For this reason, controlling the shape, like a sphere, is one of the important points. Enhancing electronic conductivity with carbon coating is the most effective way. Carbon is substantially lighter and less expensive than other coating materials like silver or copper. The goal of this experiment is to produce a nano-sized hollow sphere LFP/C structure and decorate it with graphene.

3.7. The Effect of Particle Size Refinement on $LiFePO_4$ Performance

Gaberscek et al. (Gaberscek, Dominko and Jamnik, 2007) suggest that the particle size is very important to optimize the performance of $LiFePO_4$ batteries. They believe that

the rate of electrochemical reactions can be controlled as the particle size becomes smaller. When the particle is very small (less than 70 nm), the modifier performance of $LiFePO_4$ would be to control the electrochemical reaction rather than to control diffusion. In this regard, Allen (Xia, Yoshio and Noguchi, 2006), Experimentally. The solid state method uses carbonless $LiFePO_4$ composites with a high specific surface area of 24.1 m^2/g. The discharge capacity at 5/C was reported to be 115 mA/g. It is evident, from the experimental results, that the particle size also has a substantial impact on $LiFePO_4$ electrocatalytic activity. So long as $LiFePO_4$ has a small particle size (nanoscale level) (Allen, Richard Jow and Wolfenstine, 2007), whether or not it is coated with carbon, its modifier performance will be superior to the larger $LiFePO_4$ size.

3.8. The Effect of Surface Carbon Coating on $LiFePO_4$ Performance

Surface carbon coatings can boost electronic conductivity, which significantly improves $LiFePO_4$'s electrochemical performance. Ravet et al (Whittingham *et al.*, 2005) investigated the carbon surface coating of $LiFePO_4$ for the first time in 1999. They explored two distinct ways to include carbon into the $LiFePO_4$ product. One method was to mix $LiFePO_4$ powder with a sugar solution and sinter it at 700°C. The other method was mixing the precursor with carbon and sintering it at 700°C. The carbon content in the $LiFePO_4$ synthesized by the latter technique was 1wt%. Following that, systematic research on $LiFePO_4$/C synthesis methods were carried out, including the carbon source types, total amount of carbon added to the precursor, and the structure of the added carbon, among other things.

The product's surface carbon coating improves its electronic conductivity while also successfully inhibiting the growth of $LiFePO_4$ particles. Gaberscek et al. (Gaberscek, Dominko and Jamnik, 2007)investigated the particle sizes of $LiFePO_4$ produced by several research organizations and the link between particle size and electrochemical performance. They attributed the carbon coating's enhancement to the presence of $LiFePO_4$ particle growth.

It is widely acknowledged that the carbon coating improves kinetic performance in two ways. The coated carbon, on the one hand, improves the electrical interaction between the particles. The coated carbon, on the other hand, inhibits the growth of the $LiFePO_4$ resulting nanoparticle product. Small particles in $LiFePO_4$ shorten the Li^+ diffusion channel, increasing the diffusion rate. Carbon coating significantly lowered the material's tap density, and hence its volumetric energy density (Doeff *et al.*, 2006). The key to the surface carbon coating research for $LiFePO_4$ is to get uniformly distributed and small particle size $LiFePO_4$ with the least amount of carbon.

3.9. Boosting the $LiFePO_4$ Electrode with rGO

The volumetric and gravimetric energy densities of conventional lithium ion batteries (LIBs) are decreased by the insulation separators needed to protect against short circuits, and the metal-foil current collectors that support the conductor sheets (Golubkov *et al.*, 2014; Gallagher *et al.*, 2016). Metal foils, for example, in a commercial lithium ion battery, they make up about 24% of the weight and 13% of the volume (Figure 3.3.). Increase the electroactive layer's mass loading (thickness) to minimize the volume and fractional mass of the separator and current collector , hence reducing energy density losses. However, due to insufficient lithium diffusion, concentration polarization limits the electroactive layer's electrolyte-accessible depth, limiting electrode thickness to ~100-125 μm. Thicker electroactive coatings are additionly more vulnerable to volume changes during cycling, delamination and cracking from the metal current collector. Studies are targeted at enhancing the performance of thick electrodes with large loadings of active electrode (Wood, Li and Daniel, 2015).

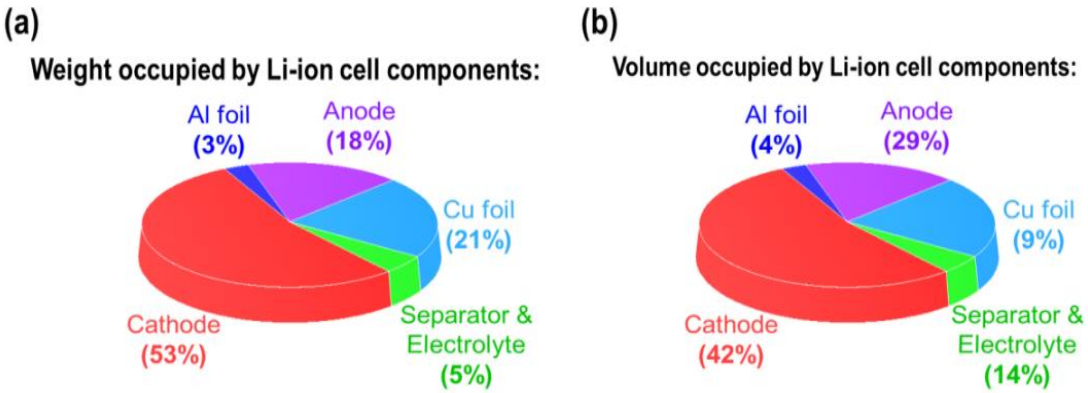

Figure 3.3. Diagram illustrating (a) mass and (b) size of a lithium ion battery's internal cell components (Golubkov *et al.*, 2014).

Instead of slurry-coated metal foil current collectors, porous, free-standing, conductive, and elastic composites with high mechanical endurance can alleviate some of these limits. This improvement minimizes the metal foil's weight and volume, and the integrated architecture allows for deformation during cycling while avoiding structural degradation (Cha *et al.*, 2018). Several other proposed electrode scaffolds made of porous metals (Abe *et al.*, 2016), elastomeric polymers (Wang *et al.*, 2011), or carbons (e.g., carbon nanotubes, graphene, etc.)(Xiao *et al.*, 2017) have been proposed in academic literature to have improved mechanical and electrochemical properties when compared to traditional metal-foil electrodes. Despite the fact that 3D composite electrodes provide compelling performance increases, their use in battery technologies has been hampered by a variety of issues: (1) long/complex synthesis methods that are difficult to scale up, (2) a limitation of processability, and/or (3) the usage of nanoscale electrode material, which result in lower active-material loadings and energy densities than metal foil cells (Cha *et al.*, 2018).

Graphene and its derivatives have emerged as prominent possibilities for 3D electrode structures due to its superior mechanical qualities, strong electrical and thermal conductivities, and wide surface area. Graphene is a two-dimensional lattice of carbon atoms that is atomically thick. These 2D "sheets" can be wrapped into 0D fullerenes, curled into 1D carbon nanotubes, or layered in 3D graphite and are the fundamental elements for graphitic materials of various dimensions (Geim and Novoselov, 2007). In commercial applications, the fundamental disadvantage of graphene

materials is the high cost and time-consuming procedures necessary to obtain high purity forms (Chabot *et al.*, 2014). Using a precursor such as graphene oxide is an effective technique to minimize these problems while keeping graphene's advantageous features (GO). GO is primarily made by oxidizing and exfoliating graphite using a method known as "Hummer's Method" (Hummers and Offeman, 1958). Hummer's method oxidizes and enhances electrostatic repulsion of graphite sheets using a highly oxidizing $KMnO_4/H_2SO_4$ solution, and when combined with rapid stirring or sonication, the graphite sheets are exfoliated, or ripped apart.

The presence of reactive groups on GO, such as carboxylic acids, hydroxyls, epoxides, and quinones, converts some sp^2-hybridized carbons into sp^3-hybridized carbons with oxygen functional groups. Even though the oxygen capabilities of GO give it a versatile reaction platform, the higher sp^3 carbon concentration reduces electrical conductivity as compared to graphite. As a result, the GO must be reduced to form reduced graphene oxide (rGO) by thermal annealing at high temperatures in an air-free atmosphere (e.g., nitrogen, argon, or ammonia) or chemical reducing agents (e.g., hydrazine, ethylenediamine, ascorbic acid, or hydriodic acid) to displace oxygen groups, restore carbon sp^2 hybridization, and increase electrical conductivity. (Kim *et al.*, 2009; Ha, Shanmuganathan and Ellison, 2015).

CHAPTER 4. EXPERIMENTAL

4.1. Raw Materials

The raw materials used to synthesize $LiFePO_4$, $LiFePO_4$/C powders are listed in Table 4.1. In this research, lithium nitrate ($LiNO_3$) was used as a source of lithium. Due to the possibility of losing lithium salt during the sintering process, the quantity of lithium content added to the precursor was optimized. And Iron nitrate ($Fe(NO_3)_3.9H_2O$) was selected as a source of iron. While Ammonium dihydrogen phosphate ($NH_4H_2PO_4$) was used as the source of phosphate ions. Glycine ($C_2H_5NO_2$) was used as a fuel. Sucrose was used as a carbon source in this work.

Table 4.1. Description of chemicals used in my master's study.

Name	Chemical formula	Vendor
Lithium nitrate	$LiNO_3$	ABCR
Iron nitrate	$Fe(NO_3)_3.9H_2O$	CARLO ERBA
Ammonium dihydrogen phosphate	$NH_4H_2PO_4$	MERCK
Glycine	$C_2H_5NO_2$	CARLO ERBA
Sucrose	$C_{12}H_{22}O_{11}$	Sigma Aldrich
Graphite	-----	Sigma Aldrich
Sulfuric acid	H_2SO_4	Sigma Aldrich
Nitric acid	HNO3	Sigma Aldrich
Sodium nitrate	$NaNO_3$	Sigma Aldrich
Potassium permanganate	$KMnO_4$	Sigma Aldrich
Hydrogen peroxide	H_2O_2	Sigma Aldrich

Table 4.1. Continue.

Name	Chemical formula	Vendor
Hydrochloric acid	HCl	Sigma Aldrich
Lithium nitrate	$LiNO_3$	ABCR
Iron nitrate	$Fe(NO_3)_3.9H_2O$	CARLO ERBA
Hydrochloric acid	HCl	Sigma Aldrich
Dimethylformamide	$(CH_3)_2NC(O)H$	Sigma Aldrich
Polyvinylidene fluoride (PVDF)	$(CH_2CF_2)_n$	Alfa Aesar
N-Methyl-2-pyrrolidone (NMP)	C_5H_9NO	Alfa Aesar
Lithium metal	Li	China
Aluminium foil	Al	China
Carbon black	C	MTI
Electrolyte	1.0 M $LiPF_6$ in 1:1 EC/DMC	China

4.2. Experiment Background

$LiFePO_4$ was prepared using solution combustion synthesis (SCS) from metal precursors of iron nitrate ($Fe(NO_3)_3 \cdot 9H_2O$), ammonium dihydrogen phosphate ($NH_4H_2PO_4$) and lithium nitrate ($LiNO_3$) in a molar ratio of 1:1:1. Glycine ($C_2H_5NO_2$) was used as a fuel. While Sucrose was used as a carbon source. Afterwards, Hummer's method was used to synthesize rGO, which was then introduced to $LiFePO_4$/C powder.

4.2.1. Solution combustion synthesis (SCS)

Combustion synthesis (CS), one of many powder synthetic processes, has recently attracted a lot of attention (Chick *et al.*, 1990; Aruna, Muthuraman and Patil, 1997). It is capable of producing a wide range of commercially viable materials with a variety of unique features at a reasonable cost. At relatively low temperatures, solution combustion synthesis (SCS) enables the successful production of a wide range of nano-

sized substances. An auto reaction that occurs in a homogeneous solution of various inorganic salts (e.g., metal nitrates) and fuels (e.g., urea, glycine). These fuels are used for two purposes: (a) They are the sources of C and H, which when burned produces CO_2 and H_2O and liberates heat, (b) They form complexes with metal ions, which allow for uniform cation mixing in solution. It has been used to successfully manufacture many electrode materials for lithium ion batteries, including $LiCoO_2$ (Julien *et al.,* 2000) and $LiMn_2O_4$ (Yang *et al.,* 1999) for the cathode and pristine or doped $Li_4Ti_5O_{12}$ (Raja *et al.,* 2009) for the anode. Another benefit of SCS is that the technique allows for simultaneous carbon coating and the production of nanostructured materials for lithium-ion batteries. A very important point, during the production of pure phase $LiFePO_4$, reduction of Fe^{3+} to Fe^{2+} must be prevented. Since Fe^{2+} is rapidly oxidized during the combustion, extracting phase-pure $LiFePO_4$ from Fe^{2+} raw materials is typically difficult. Therefore, the process must be performed in the presence of inert gases (N_2, H_2, Ar), which are necessary for reducing iron to a lower oxidation state and forming the olivine $LiFePO_4$ phase.

4.2.2. Synthesis of $LiFePO_4$

The initial stage in the experimentation will be to produce samples of $LiFePO_4$. Separately, 2.52 g $LiNO_3$, 13.5 g $Fe(NO_3)_3.9H_2O$, and 3.83 g $NH_4H_2PO_4$ are dissolved in a minimum amount of distilled water using magnetic stirrer at 300 rmp. The molar ratio of Li:Fe:PO_4 is 1:1:1. Then mixed all the solutions ($LiNO_3$, $Fe(NO_3)_3.9H_2O$ and $NH_4H_2PO_4$, respectively) one by one at the interval of 10 minutes. Then a calculated amount of glycine was added dropwise to the solution while stirring. The solution was kept stirring at 80°C at 300rpm until a gel had formed. The gel was then placed to a pre-heated oven at 150°C to produce a fluffy powder. After collecting the powder, heating it up to 700°C in a nitrogen-gas-protected tube furnace for 4 hours to get crystalline LiFePO4 powder. The method is depicted in detail in Figure 4.1.

The following equation can be used to explain the synthesis of $LiFePO_4$ via Solution combustion process (SC):

$$LiNO_3 + Fe(NO_3)_3 + NH_4H_2PO_4 + 2C_2H_5NO_2 \Rightarrow LiFePO_4 + 7/2N_2 + 4CO_2 + 8H_2O \quad (4.1)$$

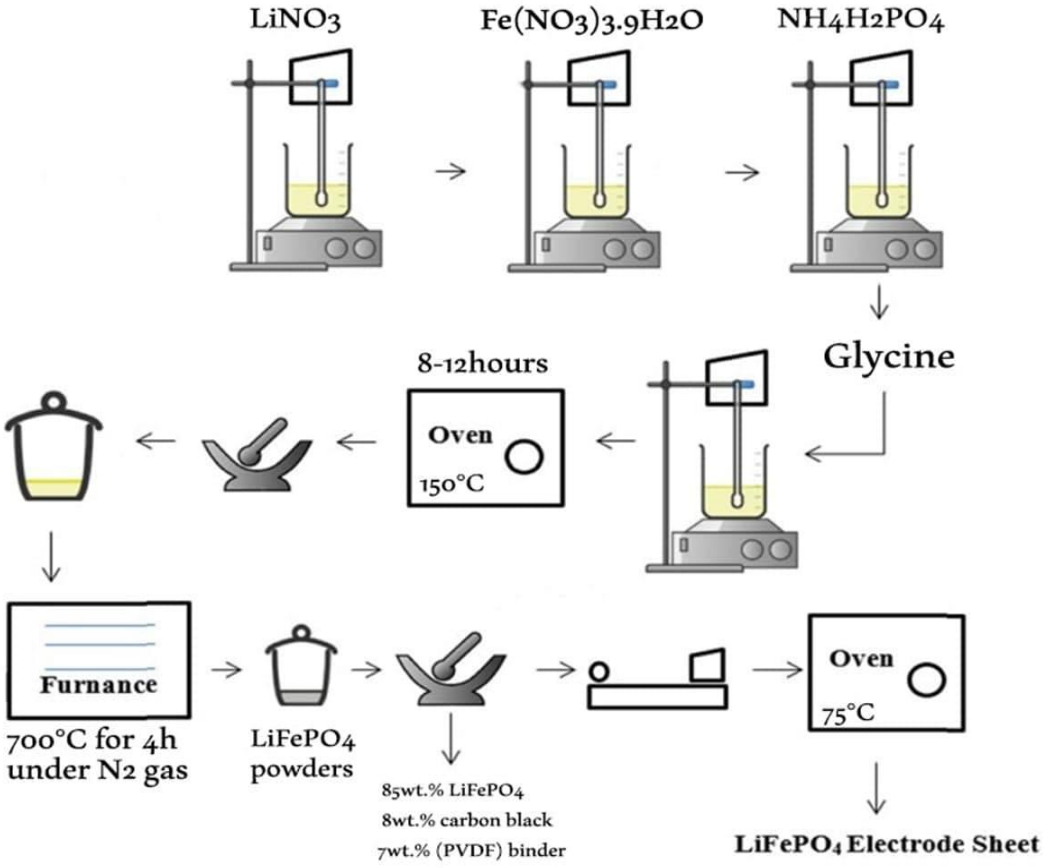

Figure 4.1. Flow diagrams of $LiFePO_4$ powder products.

4.2.3. Sucrose as a carbon source

The surface charge transfer process and surface conductivity of $LiFePO_4$ are typically improved by a carbon coating, since it has low electrical conductivity naturally. The introduction of sucrose was attempted in three different ways:

- (way1) It was added before the formation of the gel during the solution stage.
- (way2) The principal product of auto combustion was mixed in ball milling.
- (way3) It was combined with the $LiFePO_4$ that was created during the calcination at 700°C, and then burned in a nitrogen atmosphere at 700° C to help the sucrose decompose.

For a more comprehensive explanation, the results will be provided in the results and discussion section.

4.2.4. Synthesis of graphene oxide

A modified Hummers method (Hummers and Offeman, 1958) was used to synthesize graphene oxide from natural graphite. Basically, graphite powder (2g) and $NaNO_3$ (1g; >99 wt%) were mixed together, then immersed in an ice bath with concentrated H_2SO_4 (96 ml; 98 wt%). $KMnO_4$ (6g; 99.5 wt%) was added gradually with vigorous stirring, and the mixture was maintained at a temperature below 20 °C. It was then stirred in a water bath at 35 °C for 18 hours after it was taken out of the ice bath. The mixture became pasty with a brownish color during the reaction. Following that, 150 ml H_2O was progressively added to the mixture while keeping the temperature beneath 50 °C. Following dilution with 240 mL H_2O, 5 mL 30 wt% H_2O_2 dropped into the mixture, which caused the solution to turn vivid yellow and bubble. HCl aqueous solution (250 mL, 1:1 by volume) was used to filtered and washed the mixture, DI water, and ethanol (anhydrous) to get rid of additional ions after 2 hours of continuous stirring. Finally, the solid obtained was vacuum dried. This collected powder was GO. The reactions occurring are shown in Equations 4.2 and 4.3.

$$KMnO_4 + 3H_2SO_4 \rightarrow K^+ + MnO3^+ + H3O^+ + 3\ HSO_4 \quad (4.2)$$

$$MnO_3^+ + MnO_4^- \rightarrow Mn_2O_7 \quad (4.3)$$

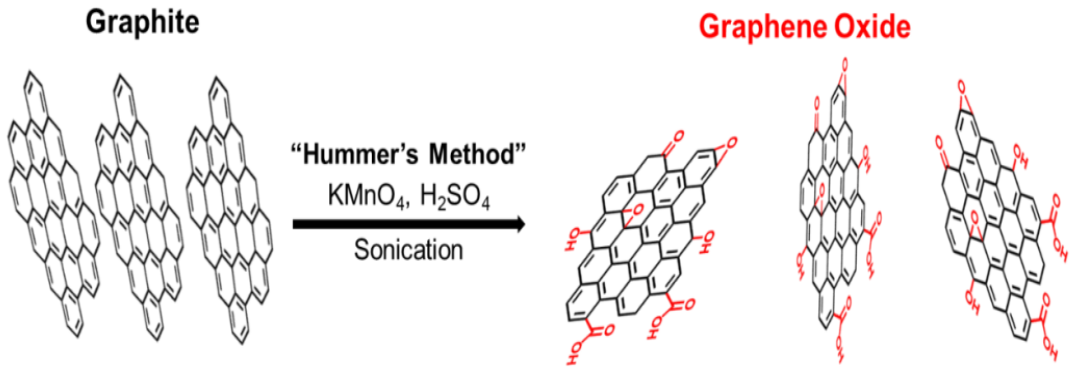

Figure 4.2. Illustration Hummer's Method for converting graphite to graphene oxide.

Thermal annealing was employed to convert synthesized GO to rGO at 800°C for 5 hours in an argon atmosphere. To prepare the colloidal solution, the pre-calculated amounts of rGO were dispersed in a DMF solution (250 p.p.m.) and sonicated for 30 minutes. After the rGO was completely dispersed, a pre-calculated amount of synthesized LFP/C was mixed into the solution and sonicated for another 30 minutes. Then moved the solution to gentle stirring at 180°C. The resultant product was dried at room temperature. The van der Waals interactions between graphene sheets and $LiFePO_4$/C particles cause the creation of graphene-wrapped $LiFePO_4$/C particles on their surfaces.

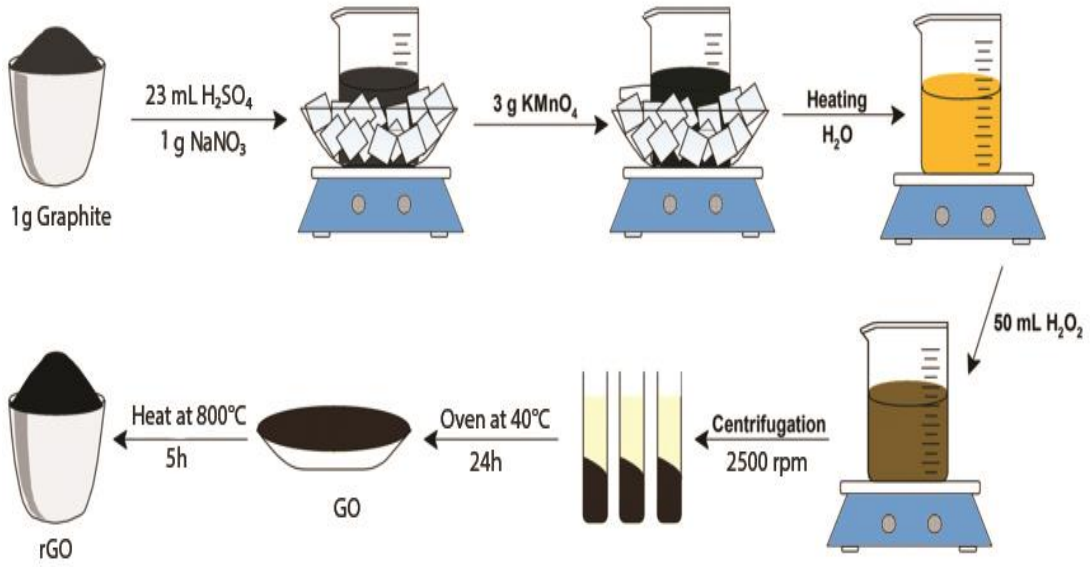

Figure 4.3. The schematic diagram of sample preparation process.

4.3. Basic Equipment Utilized

The synthesis of $LiFePO_4$/C powders includes sol-gel formation, drying, and elevated heat sintering. Figures 4.4. , 4.5. and 4.6. showed the actual setup images for sol-gel processing, drying, and high temperature sintering, respectively.

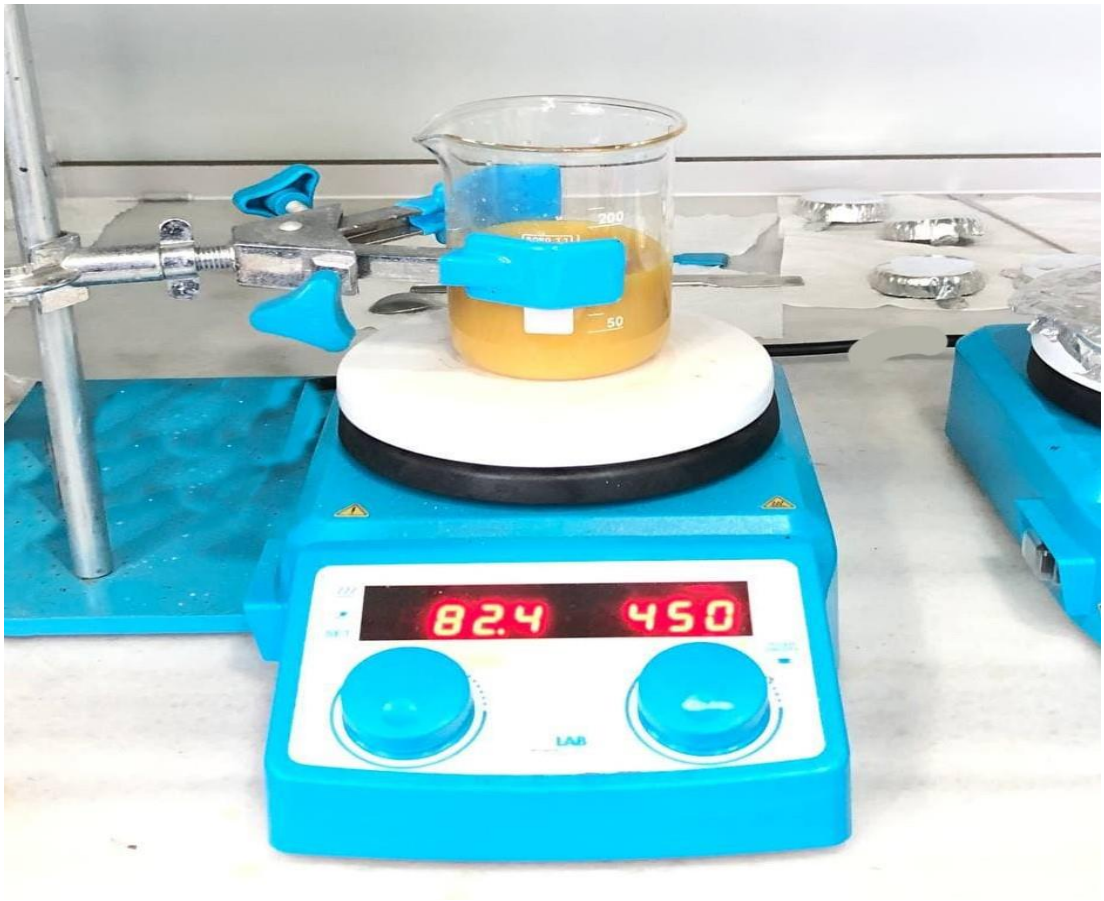

Figure 4.4. synthesize process.

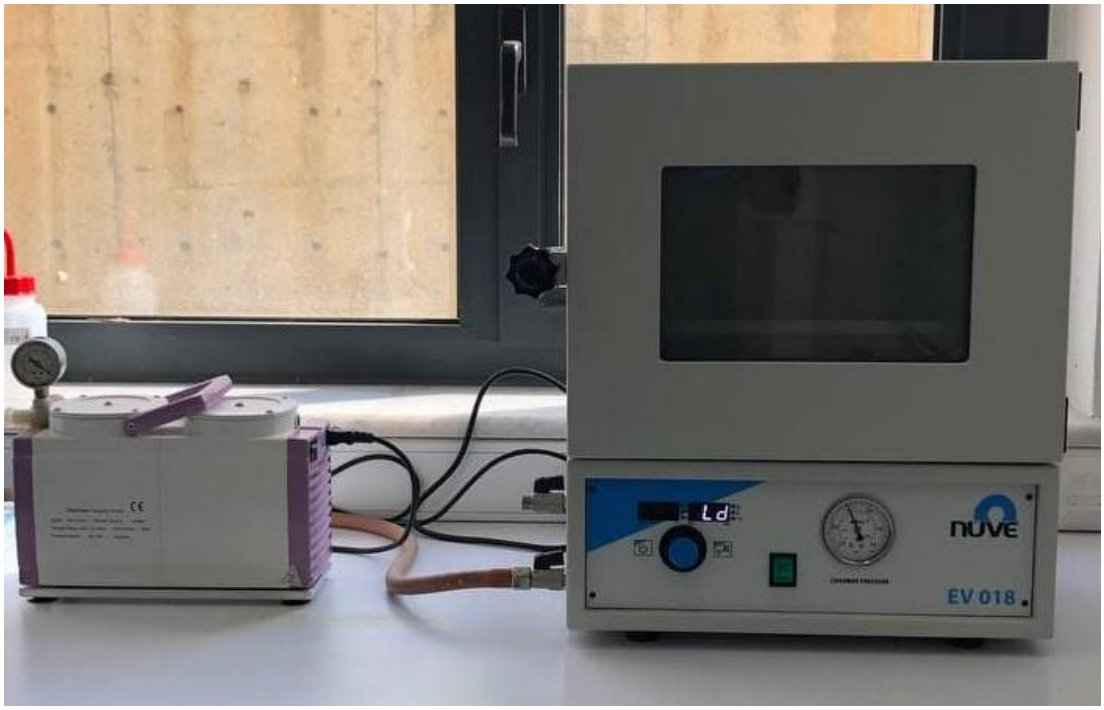

Figure 4.5. Oven.

Figure 4.6. Tube furnace for sintering the dried precursor.

4.4. Preparation of Cathode Electrode Material

The electrochemical properties of the produced $LiFePO_4$ samples were investigated using coin-shaped cells with metal lithium sheets as the reference electrode. The cells used a Li metal (–) | electrolyte | $LiFePO_4$ (+) configuration with a liquid electrolyte (1 M $LiPF_6$) electrolyte in a dimethyl carbonate (DMC) and ethylene carbonate (EC) mixed solvent of 1:1 (v/v) (EC). The separator was constructed using microporous polypropylene film (Celgard 2400). The electrochemical testing working electrodes were made by homogeneously combining 85 wt.% $LiFePO_4$ or $LiFePO_4$/C powder, 8 wt.% conductive carbon Super P and 7wt.% polyvinylidene fluoride (PVDF) binder in an N-methyl-2-pyrrolidone (NMP) solvent. The slurry was then cast onto an aluminum foil current collector (10 mm). After drying at 80°C for about 12 h, the electrode disks (14 mm) were punched and weighed. The amount of active material that was loaded

onto the electrode disks was about 2.5 mg cm^{-2}. The cells were assembled in a glove box filled with pure argon, which is shown in Figure 4.8. A glove box is a closed box that allows someone to work inside while being isolated from the outside environment.

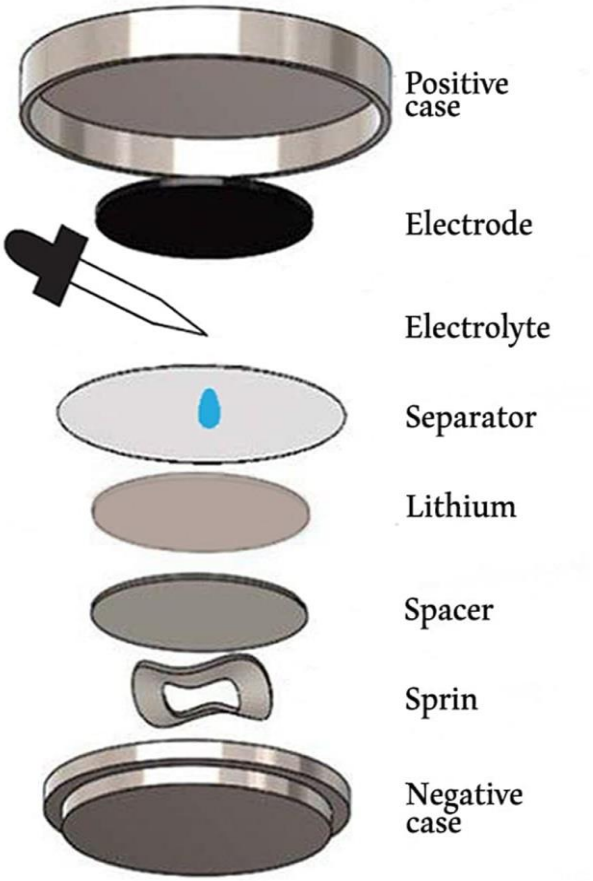

Figure 4.7. Coin cell configurations.

Figure 4.8. Glove box.

Figure 4.9. shows the cathode sludge and foil coated by the sludge in our laboratory.

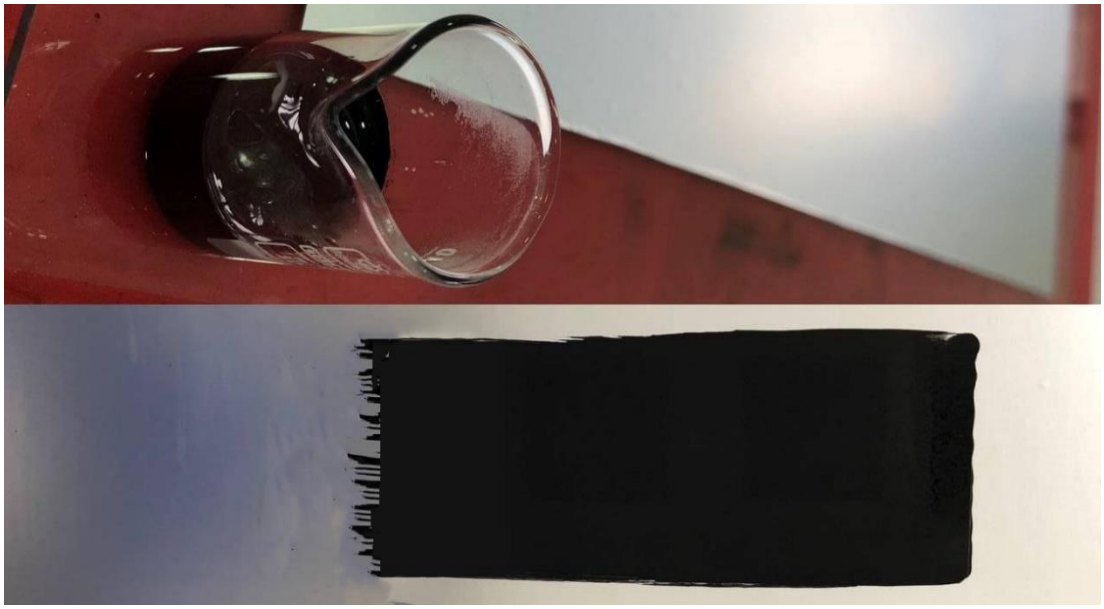

Figure 4.9. Images of electrode materials and slurry.

The size of each chip is appropriate for the coin cell battery. To compute the current of each coin cell battery, the weight of each electrode material is necessary. After cutting, each chip-shaped aluminum foil weighs 5.2 mg. So, after deducting 5.2 mg, the precise weight of electrode components should be approximated. Assemble each coin cell battery according to the coin cell assembly shown in Figure 4.7. When assembling the coin cell battery, electrolyte will be poured into the cell. Then, using the crimping machine, seal the coin cell, which is shown in Figure 4.10.

Figure 4.10. Coin cell crimping machine.

The battery test device can detect differing electric currents in coin cell batteries. The current is a parameter that must be estimated based on the cathode materials' active mass. As a result, the weight of electrode materials predicted previously can be used here. The theoretical capacity of LFP is 170 $mAhg^{-1}$ with 1C current and it shows a plateau at around 3.5 V vs. Li^{+}/Li. Calculate the current for each battery based on the actual weight of each coin cell and input it into the battery testing equipment.

The coin cell battery system, shown in Figure 4.11. is a product from the MTI vendor. We examined the charge and discharge capacities of $LiFePO_4/C$ specimens in this experiment using the following standard charge/discharge conditions: 2.5-4.3.

Figure 4.11. Coin cell battery test system.

CHAPTER 5. RESULTS AND DISCUSSION

5.1. Investigation of Fuel to Oxidant Ratio

5.1.1. Thermal analysis

A thermogravimetric analyzer was used to characterize the sample, which were burned at a rate of 10°C/minute from ambient temperature to 850°C in a nitrogen environment. The thermal behavior curves for $LiFePO_4$ sample is shown in Figure 5.1.

The TG curve of the $LiFePO_4$ sample has three stages, as shown in Figure 5.1. Water evaporation causes a modest drop in mass in the first stage, which takes happen at temperatures between 60 and 300°C. An endothermic process culminates at 227°C, which characterizes this occurrence. As a result, $LiFePO_4$ decomposition would be impossible in this temperature range. In the second part, at 325-610^{0}C, the weight increases around 3.86% with three exothermic reactions at 348^{0}C, 540^{0}C and 605^{0}C. This reaction is an oxide decomposition of amorphous $LiFe^{II}PO_4$ into $Li_3Fe_2(PO_4)_3$ and Fe_2O_3, as described in the reaction below:

$$LiFe^{II}PO_4 \text{ (amorphous)} + ¼\ O2 \rightarrow 1/3\ Li_3Fe_2{}^{III}(PO4)_3 + 1/6\ Fe_2{}^{III}O_3 \quad (5.1)$$

In order to continue oxidation of $LiFePO_4$, the following stage is a continuous plane with little weight loss. This result is consistent with that obtained by others, in which that olivine $LiFePO_4$ oxidizes to $Li_3Fe_2(PO_4)_3$ and Fe_2O_3 at temperatures varying from 250 to 550 °C. without the presence of any other compounds that protect LiFePO4, even when 30 mL/min N_2 is still flowing. The third stage is at 510-750°C, where the weight drops by 4.8% due to carbon oxidation into CO_2, leaving the $LiFePO_4$ coupled with the excess carbon. The carbon content of $LiFePO_4$ was estimated using the formula: total carbon contributed minus burned carbon = leftover carbon. In this case,

the carbons that remain active in the material are 5%-4.8% = 0.2%. It is obvious from this decomposition behavior that carbon's role in the calcination process is primarily to protect $LiFePO_4$ from oxidation.

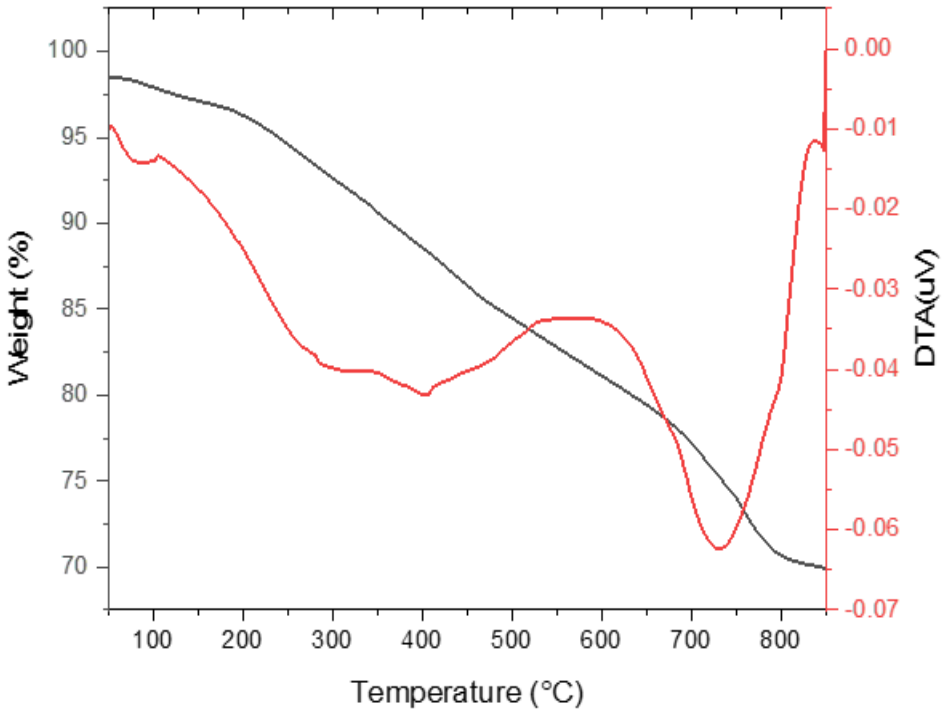

Figure 5.1. Thermal analysis curve of $LiFePO_4$ powder produced by combustion technique in a N_2 environment at a heating rate of 10°C/minute.

5.1.2. Structural analysis of $LiFePO_4$

Using Fe(III) as the raw substance and conducting the combustion synthesis in the open atmosphere, the fuel to oxidant proportion within the reactant mixture will indeed ascertain the structure and the combustion temperatures of the surrounding atmosphere during the combustion process, that further could impact the formation of the $LiFePO_4$ phase. As a result, different fuel to oxidant ratios were investigated. The fuel to oxidant ratio was represented by the molar ratio of glycine to $LiFePO_4$ (x) for simplicity. The matching products were designated x-LFP, and the ratio (x) was chosen to be 1, 2, 4, 5, and 6. Color variations were observed in the primary products of auto combustion. Samples 1LFP and 2LFP took on the color brown, indicating the existence of a Fe_2O_3 phase. It shows that during the combustion process, at least some iron (III)

in the reactants was not reduced to Fe^{+2}. The color changed to dark grey with a further rise in fuel to oxidant ratio, indicating that the majority of Fe^{+3} had been successfully reduced after auto-combustion. Since the direct combustion samples showed poor crystallization and a considerable proportion of restriction organics, they were all calcined in nitrogen gas for 4 hours at 700 °C. The XRD patterns of the various products following calcination are shown in Figure 5.2. The olivine $LiFePO_4$ phase diffraction peaks were visible in samples 1LFP and 2LFP. There are also high intensity diffraction peaks at 24.4° and 33.3°, corresponding to Fe_2O_3 diffraction planes [101] and [112], and low intensity peaks at 26.7° and 27.5°, corresponding to $Li_3Fe_2(PO_4)_3$ phase diffraction planes [113] and [122], were also detected. These results indicated that the ferrous in those specimens was predominantly in the Fe(III) form, which corresponded to the primary products' brown color. The olivine $LiFePO_4$ phase appears to dominate most of the diffraction peaks in sample 4LFP, unless there are a few weak diffraction peaks with a very low intensity around 40°, possibly attributed to the form of iron phosphocarbides, iron carbide, or iron phosphides. Further peaks appear at 40.3°, 44.2°, and 47.2° correspond to the Fe2P phase, with incidence planes of [111], [210], and [201], respectively, as the amount of fuel increased, i.e. for sample 5LFP, in addition to the olivine $LiFePO_4$ phase, whereas for sample 6LFP, the olivine phase was almost absent, with Fe_2P as the dominant phase. It indicates that the samples were too reduced at those high fuel to oxidising agent ratios.

Theoretically, the most stable gaseous products are CO_2, N_2, and H_2O. $LiNO_3$ and $Fe(NO_3)_3$ act as oxidising agents, meanwhile $NH_4H_2PO_4$ and glycine act as fuels. This indicates that at a fuel-to-$LiFePO_4$ ratio (x) of 2:1, the combustion may be self-sufficient, requiring no external oxidant (O_2). The fuel stoichiometric condition describes this circumstance. If x is less than 2, there isn't enough fuel to completely reduce the oxidant, and the system is in a fuel-deficient state. If x is more than 2, Nevertheless, It is running on a lot of fuel. In principle, at x of 2, the Fe(III) must be entirely converted to Fe(II); but, since the combustion took place in the open air, oxygen from the atmosphere likewise also participated in the combustion process, consuming some glycine fuel, putting the reactor in a fuel-insufficien state. It therefore

clarifies why some unreduced Fe(III) is present in the initial product of auto combustion at x = 2.

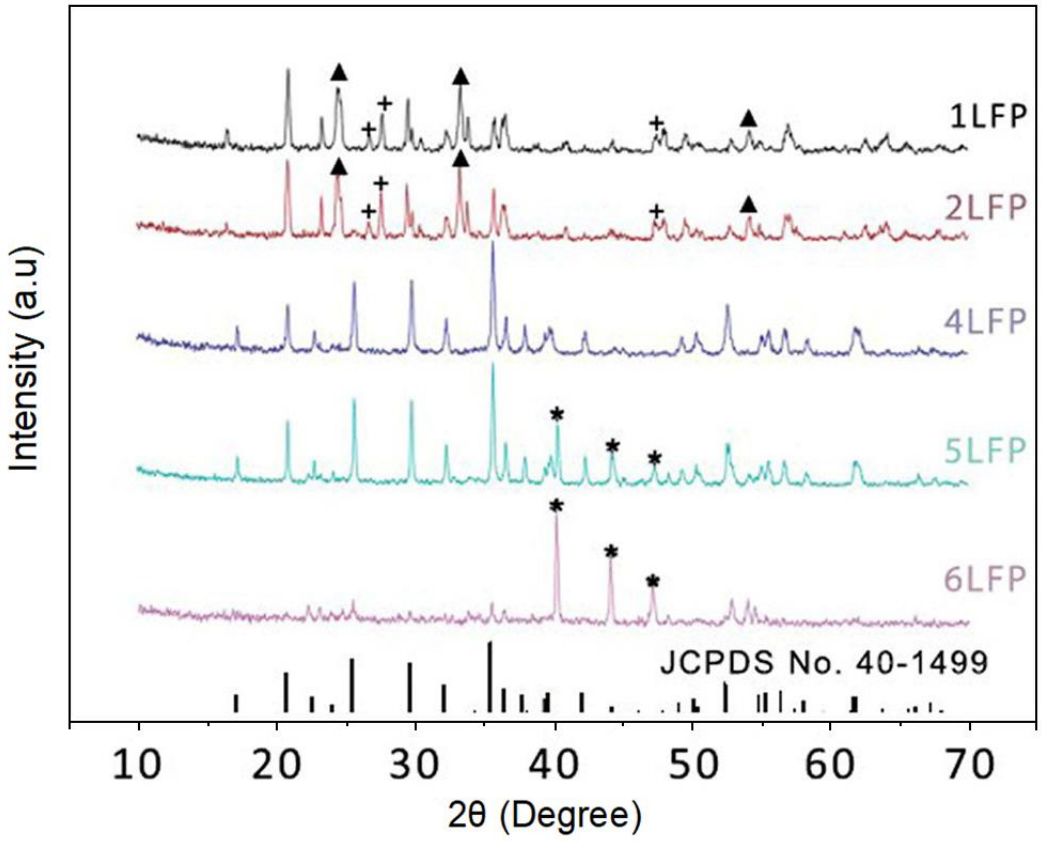

Figure 5.2. The XRD patterns of $LiFePO_4$ powders synthesized with various quantities of glycine (▲: Fe_2O_3, +: $Li_3Fe_2(PO4)_3$; *: Fe_2P).

5.1.3. Morphology of $LiFePO_4$

Figure 5.3.(a),(b) displays FESEM pictures of as-prepared $LiFePO_4$ powders with the optimal glycine to $LiFePO_4$ ratio. The sample was made up of agglomerated particles, as illustrated in the photos. The grain size of sample 4LFP was on the level of several micrometers, indicating that the particle size was significantly sintered. The EDS analysis (Figure 5.3.(c)) suggests that the 4LFP sample contain about 0.83%C.

The component distribution is shown by EDS mapping of the FESEM. Figure 5.4 depicts the EDS mapping of a single particle with a carbon sheet substrate. The

element scanned are iron, phosphorus, oxide and carbon. Lithium cannot be scanned using FESEM since it's too weak. EDS mapping further confirms the successful incorporation of LFP.

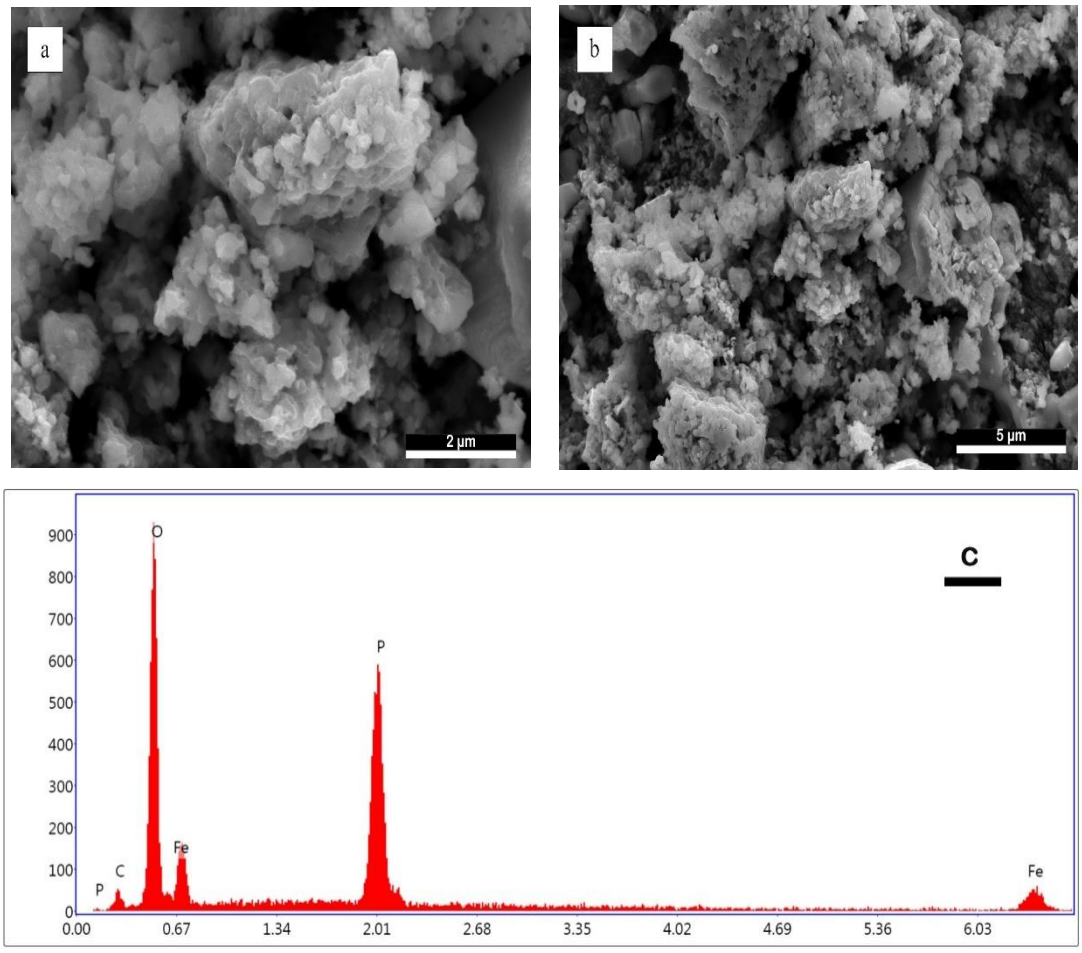

Figure 5.3. (a) and (b) FESEM images of the 4-LFP sample at various magnifications, (c) EDS of the 4-LFP.

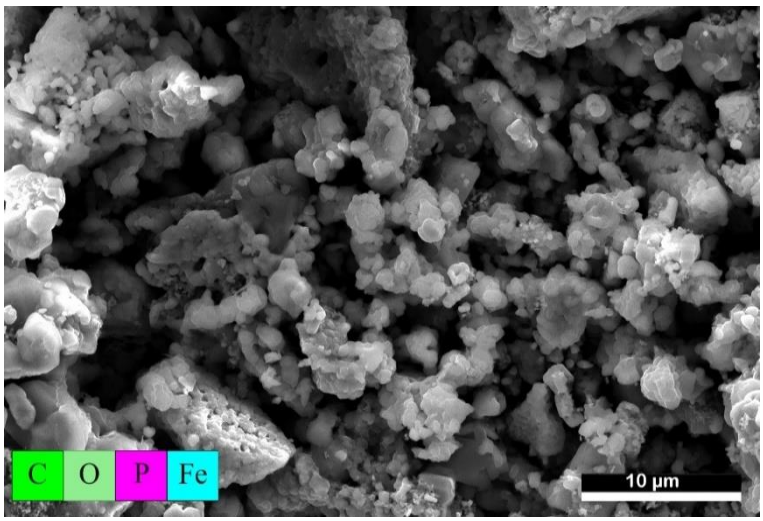

Figure 5.4. EDS mapping images of 4-LFP.

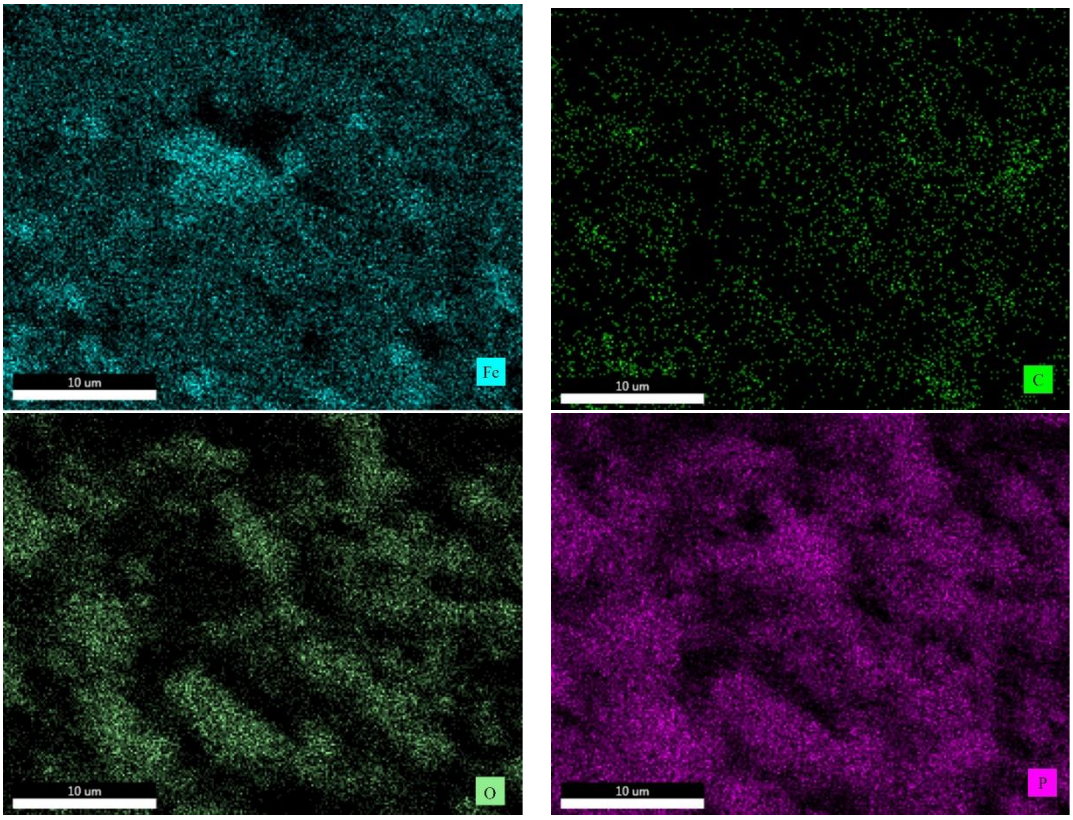

Figure 5.4. Continue.

5.1.4. Electrochemical performance of LiFePO4

5.1.4.1. Charge discharge properties

Figure 5.5. depicts the charge-discharge curves of the various products at a 0.1 C rate. The capacity of The capacities of specimens 1LFP and 2LFP were just 5 and 22 mAh/g, respectively. 1LFP and 2LFP was only 5 and 22 mAh/g, respectively. Furthermore, there was no discharge and charge highlands, which is consistent with weak olivine $LiFePO_4$ phase formation, as shown by XRD in Figure 5.2. The discharge capacity improved considerably to 102 mAh/g when the glycine to $LiFePO_4$ weighed amount was raised to 4:1 (x = 4), and discharge-charge highlands at 3.39 and 3.45 V were clearly apparent, which is compatible with the production of well olivine phase, as shown in Figure 5.5. The discharge capacity of the sample (5LFP) was dropped to roughly 73 mAh/g as x was increased to 5. For sample 6LFP, it was reduced to around 38 mAh/g. Meanwhile, the discharge highlands were constant in both samples (5LFP and 6LFP). The significant reduction of iron (III) during the synthesis of Fe_2P,

according to the XRD data, likely reduced the concentration of $LiFePO_4$ in the compounds, resulting in decreased charge-discharge capacities. The results showed that a sufficient fuel-rich environment was crucial for the high-capacity synthesis of pure phase $LiFePO_4$ from Fe(III) raw material via solution combustion synthesis.

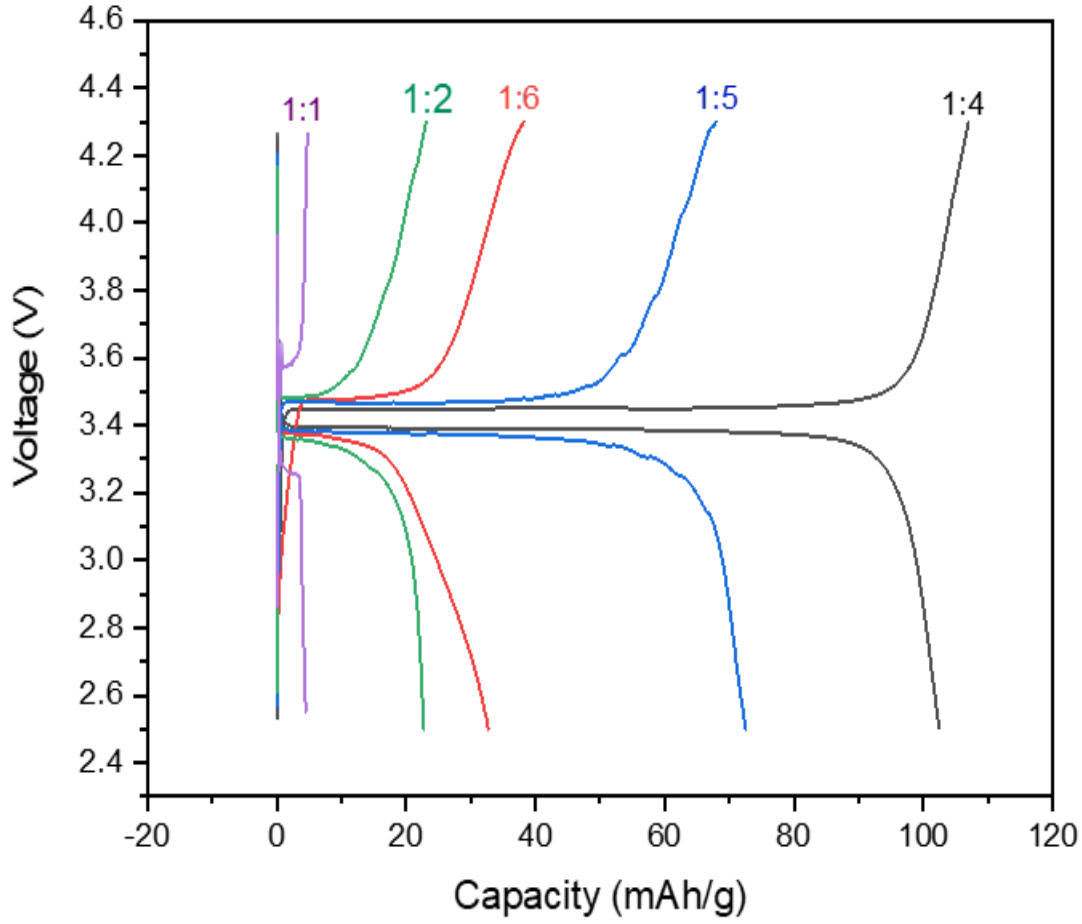

Figure 5.5. The voltage profiles for the first cycle charging and discharging (with a rate of 0.1 C) for different $LiFePO_4$ samples synthesized with varied glycine concentrations at a 0.1C rate.

5.1.4.2. Cyclic voltammetry (CV)

The CV curve of the $LiFePO_4$ sample with the glycine ratio of 1:4 at at 0.1 mVs^{-1} in the voltage range 2.5–4.5 V are shown in Figure 5.6. The area of the curve represents the charge and discharge capacity of a battery. The oxidation peak is located in the upper half of the curve, corresponding to the charging process. Whereas the lower half peak is the reduction peak, corresponding to the discharging process. When the battery

is in the charging status, the voltage increase from 2.5V to 4.5V. Li-ions delithate from the $LiFePO_4$ structure, portion of the $LiFePO_4$ becomes $FePO_4$, with an oxidation peak voltage of 3.7V. And when the voltage scan returns from 4.5V to 2.5V, indicating that the battery is discharging, The voltage corresponding to the reduction peak is 3.23V, as Li ions lithiate back into the $LiFePO_4$ structure. The polarization between the electrodes is reflected in the distance between the peaks of oxidation and reduction. The larger the gap, the higher the polarization. Therefore, the deviation of the actual potential will be larger than the equilibrium potential. On the contrary, the smaller the polarization, the narrower the gap. Therefore, the deviation of the actual potential will be lower than the equilibrium potential. As we can see in the figure, the oxidation and reduction peaks are identical in form and exhibit high symmetry. The oxidation peak to reduction peak ratio is 0.31, indicating that this material has good lithiation/delithiation reversible ability. Its oxidation peak and reduction peak barely changed in shape after 10 cycles. This demonstrates that the material has good cyclic reversibility.

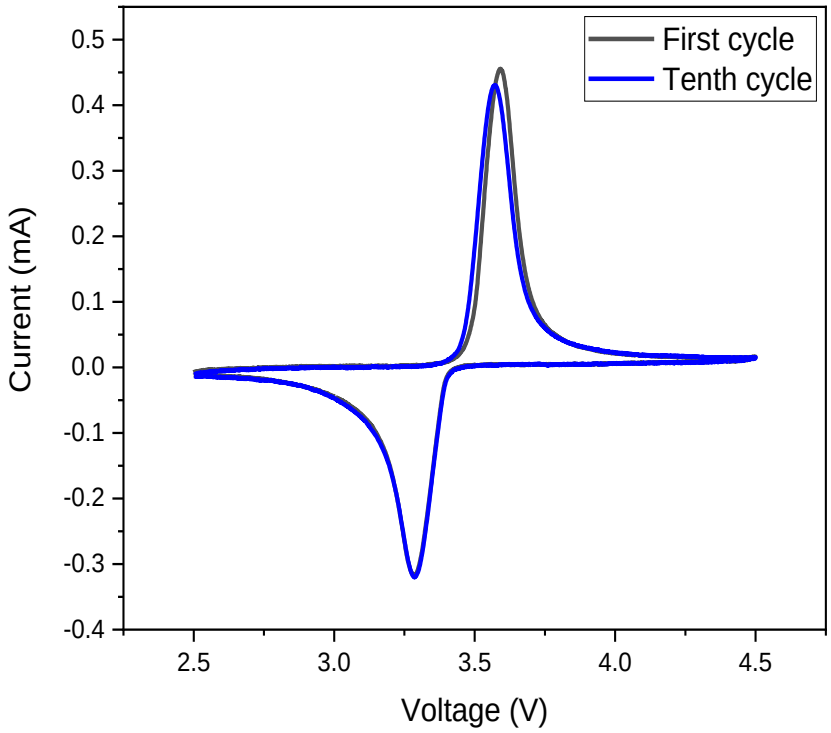

Figure 5.6. Cyclic voltammetry curves of $LiFePO_4$ with the glycine ratio of 1:4 first and tenth cycles at 0.1 mV/s .

Figure 5.7. is the CV curves of $LiFePO_4$ at different scan rates. The redox peak currents will increase when the scan rate is increased, as seen in the figure. In addition, when the scan rate increases, the potential differentiation among both the oxidation and reduction peaks also increases. This indicates that as the scan rate is increased, the polarization of this material becomes larger. When the scan rate is increased, polarization during the charge transfer process causes the oxidation peak to shift to the high potential areas, meanwhile the reduction peak moves to the low potential areas.

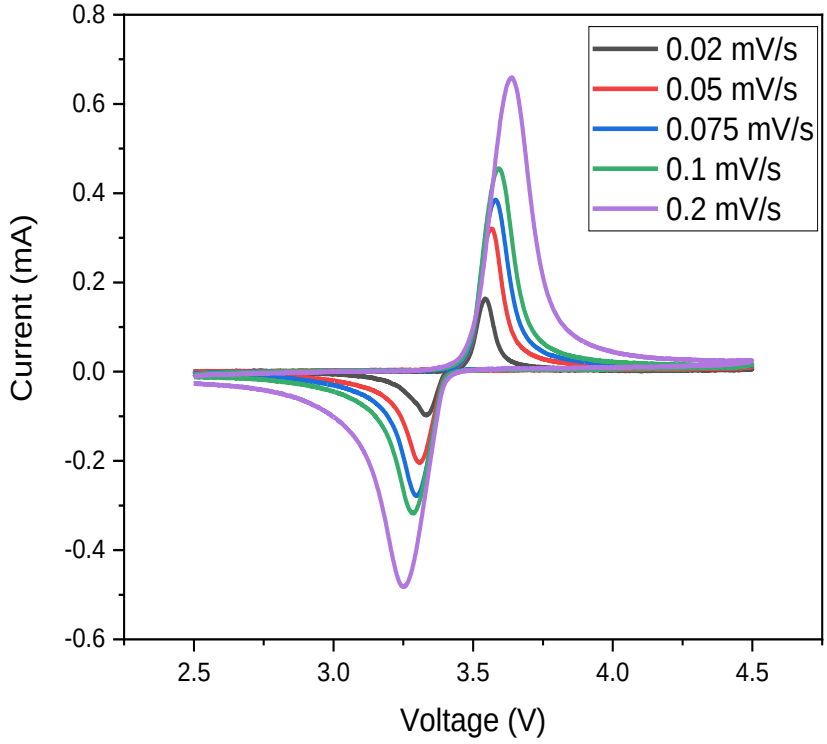

Figure 5.7. Cyclic voltammetry curves of $LiFePO_4$ with the glycine ratio of 1:4 at different scan rates (from inner to outer: 0.02, 0.05, 0.075, 0.1, 0.2 mV/s).

5.2. Carbon Coated of $LiFePO_4$

The theoretical gravimetric capacity of the olivine $LiFePO_4$ phase is around 170 mAh/g. However, the sample synthesized using combustion synthetic at the desirable glycine-to-$LiFePO_4$ ratio of 4:1, that included approximately 0.83 wt. percent carbon, had a maximum discharge capacity of just 102 mAh/g at a 0.1 C rate, as previously demonstrated. Since $LiFePO_4$ has a low electrical conductivity by nature, a carbon

coating is usually used to increase the conductivity of surfaces as well as the process of surface charge transfer. Obviously, the sample 4LFP's carbon content of 0.83 wt% is insufficient. Although increasing the fuel (glycine) to oxidant ratio can enhance carbon content, it also causes iron overreduction and the formation of Fe_2P. Consequently,, capacity was reduced. The mass ratio of glycine to LiFePO4 (x) equaled 4 was chosen since the principal product from auto combustion had the fewest contaminant phases. The introduction of sucrose was attempted in three different ways. The $LiFePO_4$ sample synthesized without sucrose was named 4LFP, whereas samples synthesized with sucrose via way1, way2, and way3 were named as 4LFP1, 4LFP2, and 4LFP3, respectively. The overall calcination time for samples 4LFP, 4LFP1 and 4LFP2 at 700° C in a nitrogen environment was kept constant at 5 h since the sintering degree is significantly connected to calcination time. For sample 4LFP3, which should be calcined twice at 700°C, different calcination times were tried.

5.2.1. Structural analysis of $LiFePO_4$/C

Sucrose decomposition was carried out in a complicated manner. In the synthesized $LiFePO_4$/C composite, different decomposition mechanisms could produce various levels of carbon, and that would have an effect on its electrochemical performance.
Figure 5.8. illustrates the XRD patterns of the four samples. Interesting to note is that samples 4LFP, 4LFP2 and 4LFP3 showed excellent olivine $LiFePO_4$ structures, while sample 4LFP1, showed an obvious Fe_2P phase, while sample 4LFP1, showed an obvious Fe2P phase, which was created from the addition of sucrose during the solution process. The sucrose also served as fuel during the combustion process after it was introduced in the solution stage. The fuel-rich situation resulted in larger concentrations of reducible CO and H_2, as well as higher combustion temperatures, both of which resulted in the overreduction of Fe(III) throughout the combustion process.

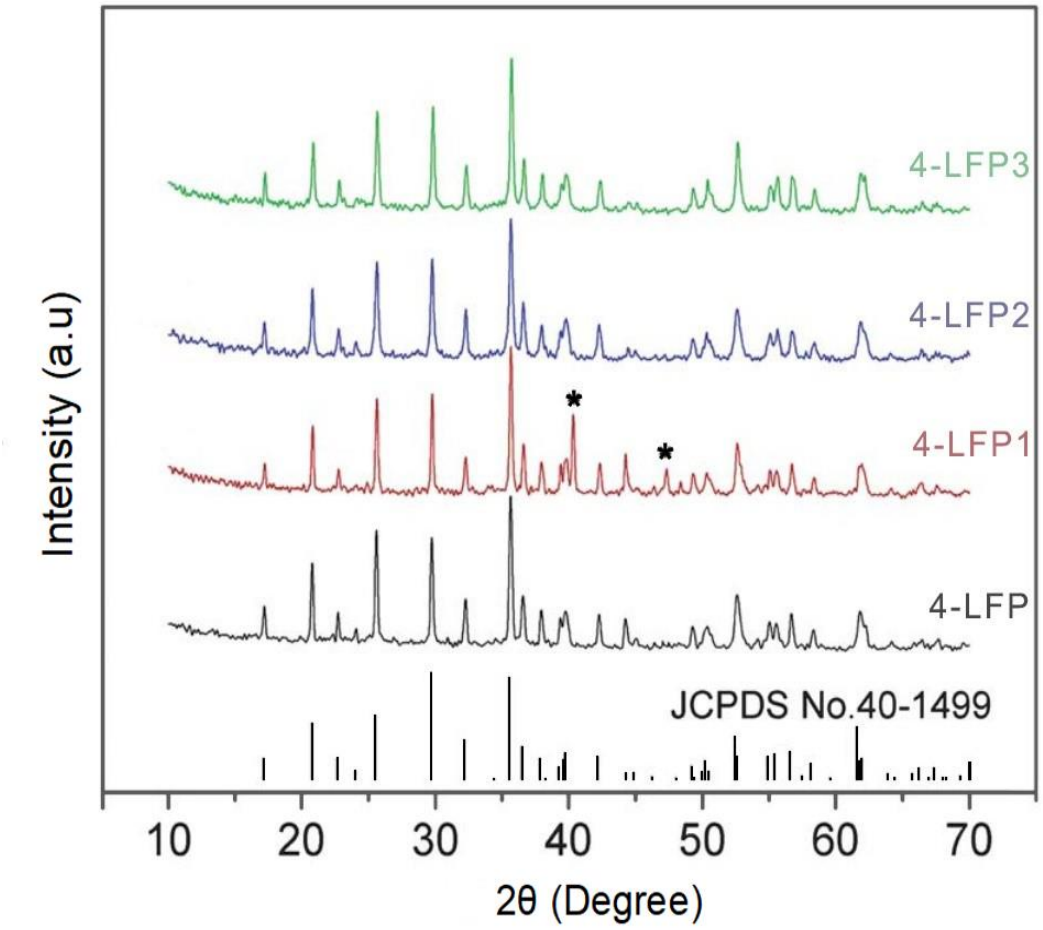

Figure 5.8. $LiFePO_4$ XRD patterns, produced by multiple sucrose introduction methods (*: Fe2P) for four different samples (4LFP, 4LFP1, 4LFP2 and 4LFP3)(*: Fe_2P).

5.2.2. Morphology of $LiFePO_4$/C

Figure 5.9.(a) and (b) are the FESEM pictures of $LiFePO_4$/C prepared by way3. From Figure 5.8.(a) shows that the material has a high magnitude of agglomerations. The material the material contains uniformly distributed nanoparticles with size of particles smaller than 1 μm, as illustrated in the high magnification image in Figure 5.9. (b). The particles are virtually spherical, going to lead a considerable increase in the interface's specific surface area. A thin carbon coating coats the surface of the particles, resulting from the in-situ decomposition of sucrose at high temperatures.The carbon layer that is coated on the top of $LiFePO_4$ may significantly improve electrical connection between the nanoparticles. To facilitate Li ion and electron transport in the

active substances, resulting in better utilization of $LiFePO_4$. The EDS analysis (Figure 5.9.(c)) suggests that the $LiFePO_4$/C sample contain about 3.4% C.

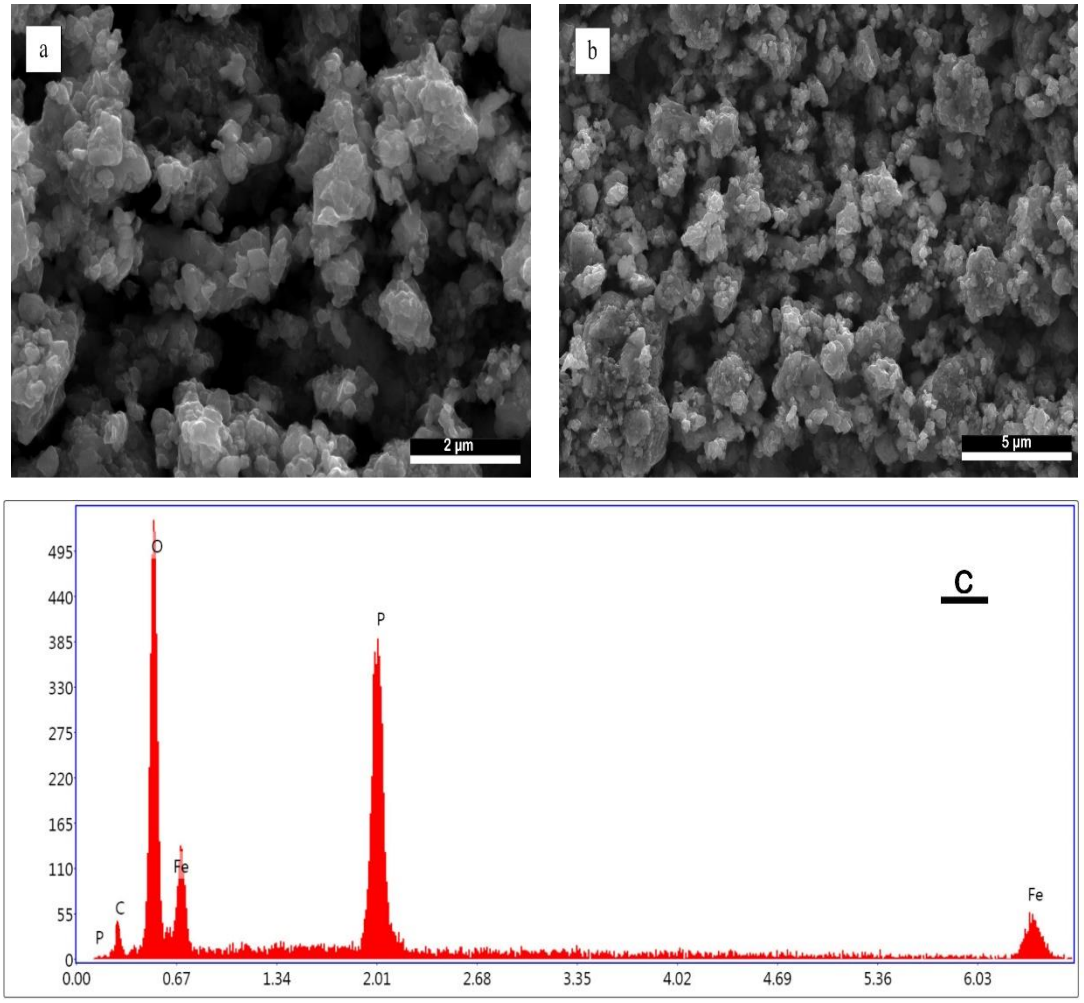

Figure 5.9. (a) and (b) FESEM images of the $LiFePO_4$/C sample prepared by way3, (c) EDS of the $LiFePO_4$/C.

Figure 5.10. depicts the elemental mapping produced with FESEM-EDS analysis for $LiFePO_4$/C generated by method 3. The pictures of the elements Fe, P, O, and C are almost identical to the matching FESEM image, demonstrating the sample's homogeneous chemical composition.

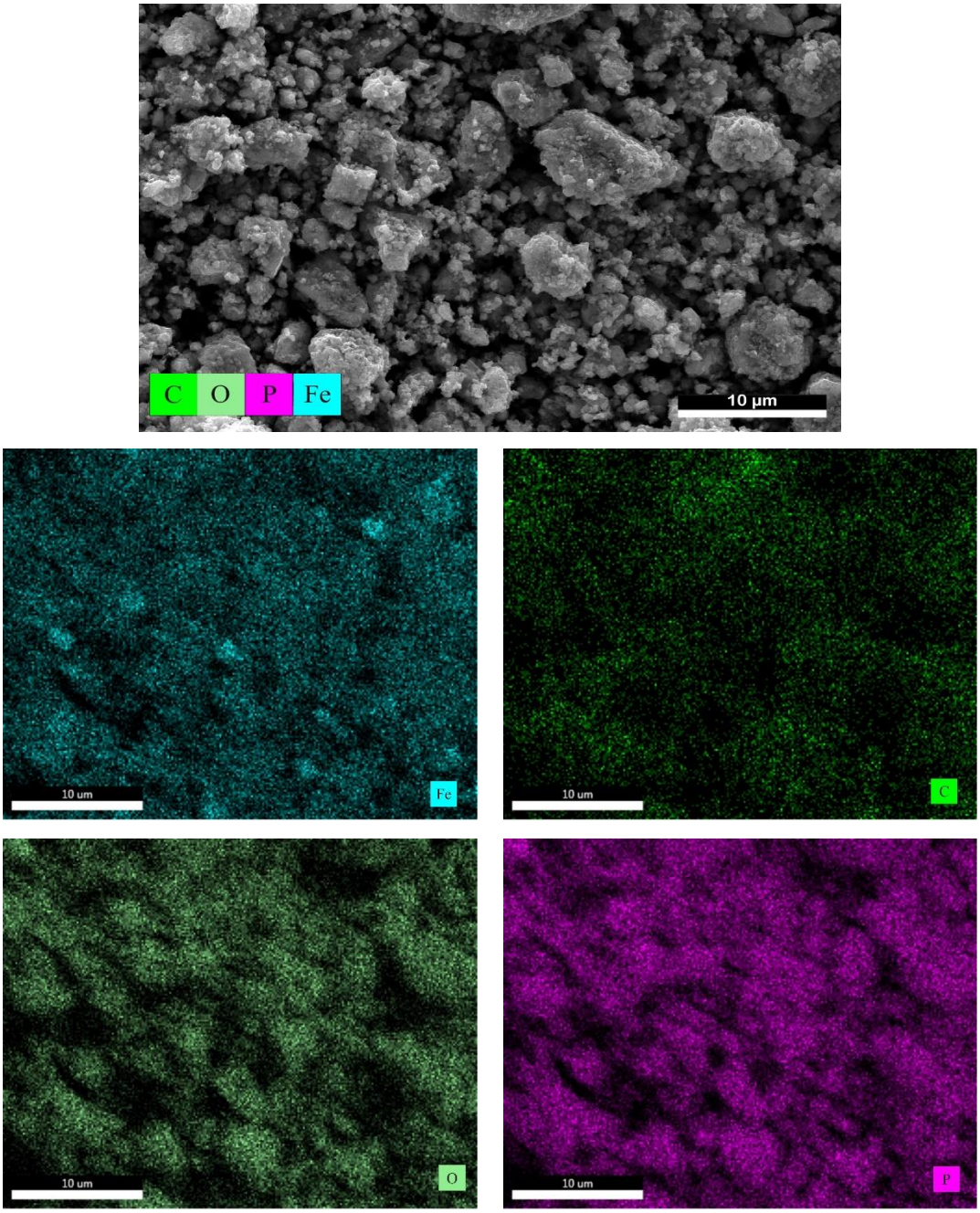

Figure 5.10. EDS mapping images of $LiFePO_4/C$.

5.2.3. Electrochemical performance of $LiFePO_4/C$

The electrode performance of various $LiFePO_4/C$ samples was first evaluated by evaluating their capacities at various rates, the results of which are shown in Figure 5.11. At a 0.1 C rate, the discharge capacities of the 4LFP, 4LFP1, 4LFP2, and 4LFP3 electrodes were 100, 102, 121, and 143 mAh/g, respectively. At higher rates, sample

4LFP3 demonstrated a substantially larger capacity than the others. At a 12 C rate, it reached 72 mAh/g, compared to 27 mAh/g for 4LFP and 13 mAh/g for 4LFP1 at the exact rate.

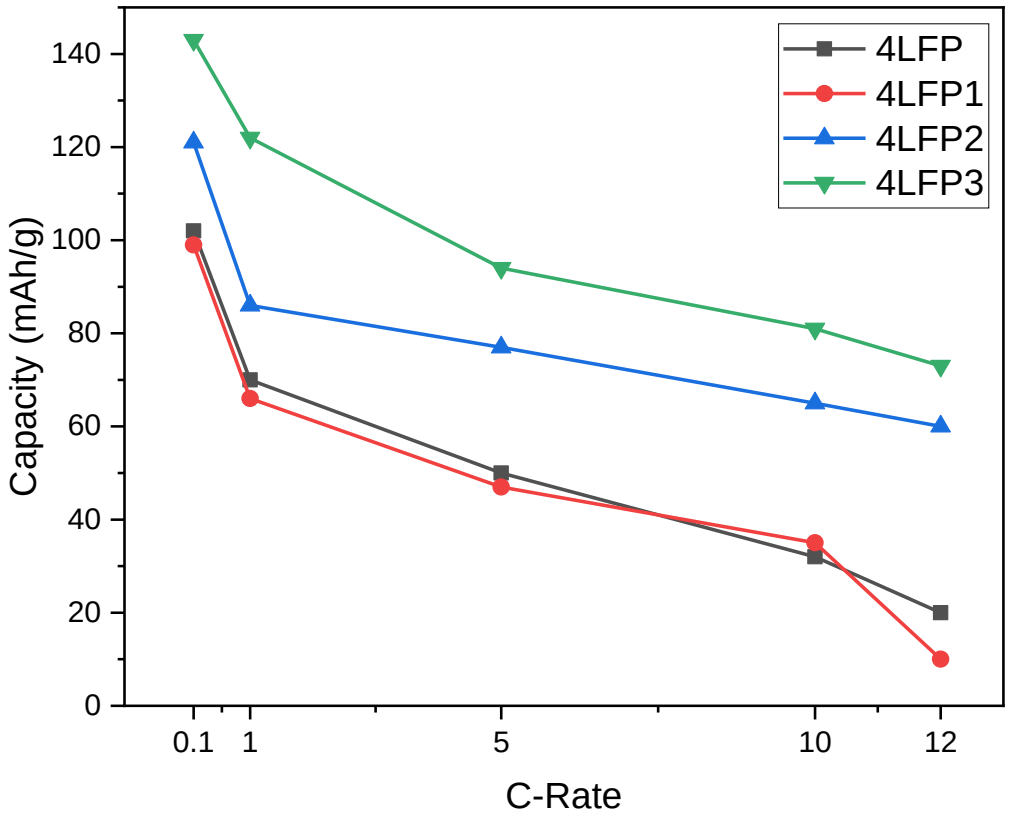

Figure 5.11. The discharge capacity of the $LiFePO_4$/C samples was compared based on the various sucrose introduction methods (4LFP1, 4LFP2, and 4LFP3).

The data on impedance backed up this conclusion. Figure 5.12. depicts the EIS of the $LiFePO_4$/C composite electrodes in a Characteristic curve. In the high to medium frequency range, all of the profiles had a depressed semicircle, and in the low frequency range, all of the profiles had an inclined line with a constant angle to the real axis. The semicircles showed a high-frequency intercept, indicating the electrolyte's ionic conductivity. The resistance associated with charge transfer between the electrolyte and the active material may be observed at lower frequencies. A third zone formed at extremely low frequencies, exhibiting classic Warburg behavior associated with lithium ion diffusion in the cathode active material. A smaller numerical value of the semicircle diameter along the Z_{re} axis is related with reduced

charge transfer resistance (R_{ct}) and, as a result, improved lithium reaction kinetics. As demonstrated in Figure 5.12., sample that synthesized by way3 had the shortest R_{ct}, followed by sample with way 2, with sample that synthesized by way1 having the biggest.

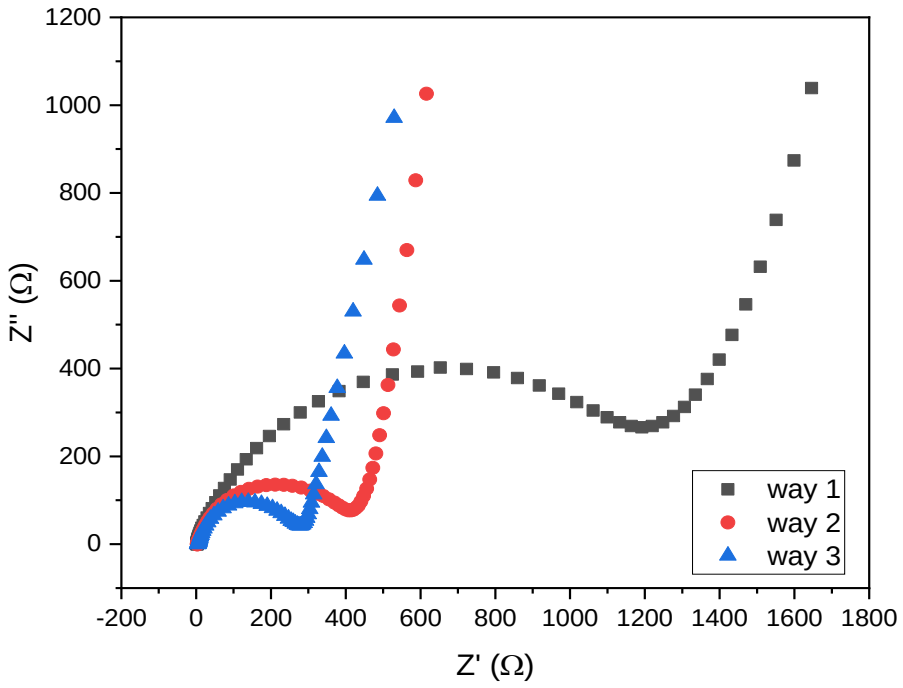

Figure 5.12. A variety of sucrose introduction methods were used to obtain EIS of $LiFePO_4$ electrodes.

As previously established, the powder made using method-3 performed the best. Nevertheless, at 0.1 C, its capacity was only 143 mAh/g, compared to the predicted value of 170 mAh/g. It implies that the carbon concentration remains inadequate. Various amounts of sucrose were employed during the synthesis to determine the required carbon content..:

The steady initial charge-discharge curves of the $LiFePO_4$/C electrode constructed according to method-3 with carbon concentrations of 10, 12, and 15% are shown in Figure 5.13. The discharge capacity was around 148, 157, and 140 mAh/g at a 0.1 C rate, respectively. The greatest capacity was reached at a 0.1 C rate with a carbon content of approximately 12wt.%. In $LiFePO_4$/C (II), the actual $LiFePO_4$ capacity was

157 mAh/g, which was close to the theoretical value of 170 mAh/g. It means that $LiFePO_4$ (II) is virtually totally electrochemically active.

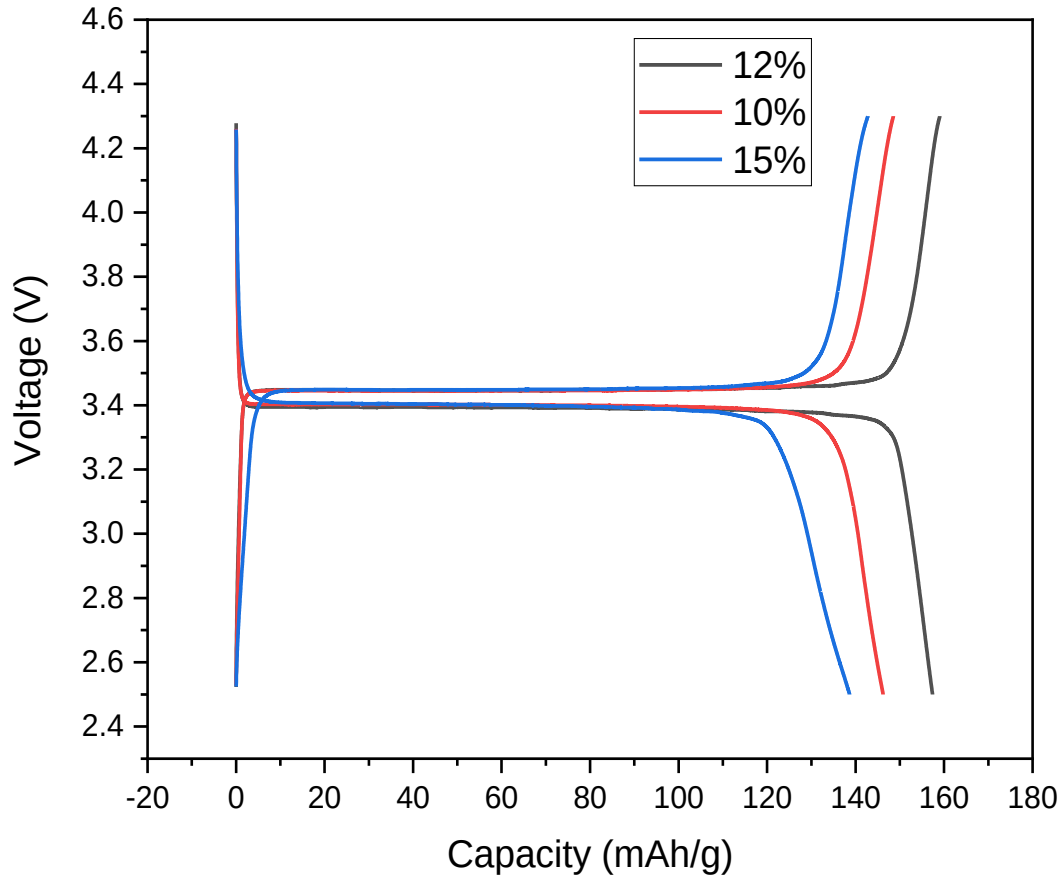

Figure 5.13. The voltage profiles of charging and discharging (at a rate of 0.1 C) based on various carbon contents.

The carbon content of $LiFePO_4$ has a significant impact on its discharge capacity. If the carbon concentration is excessive, the surface carbon will be thicker, making it easier to obstruct the movement of electrolyte and Li ions. Carbon, on the other hand, is a non-active material. The volumetric energy density will decrease as the carbon concentration increases. As a result, the carbon content should be as low as possible as long as it is sufficient to coat the active substances.

The CV profiles of the $LiFePO_4$/C sample obtained by method 3 are shown in Figure 5.14. There are two types of peaks: oxidation and reduction. These peaks are caused by a multiple interaction between the lithiated phase, $LiFePO_4$, and the delithiated

phase, $FePO_4$. The potential difference between the cathodic (3.75V) and anodic (3.1V) peaks, on the other hand, is 0.65V. During the redox process, the gap among both the cathodic and anodic peaks (0.65V) shows a smaller polarization potential. Furthermore, the oxidation/reduction peaks are sharp and symmetric, indicating that the lithium intercalation and de-intercalation processes are reversible and electrochemically active. Its oxidation peak and reduction peak barely changed in shape after 10 cycles. This demonstrates that the material has good cyclic reversibility.

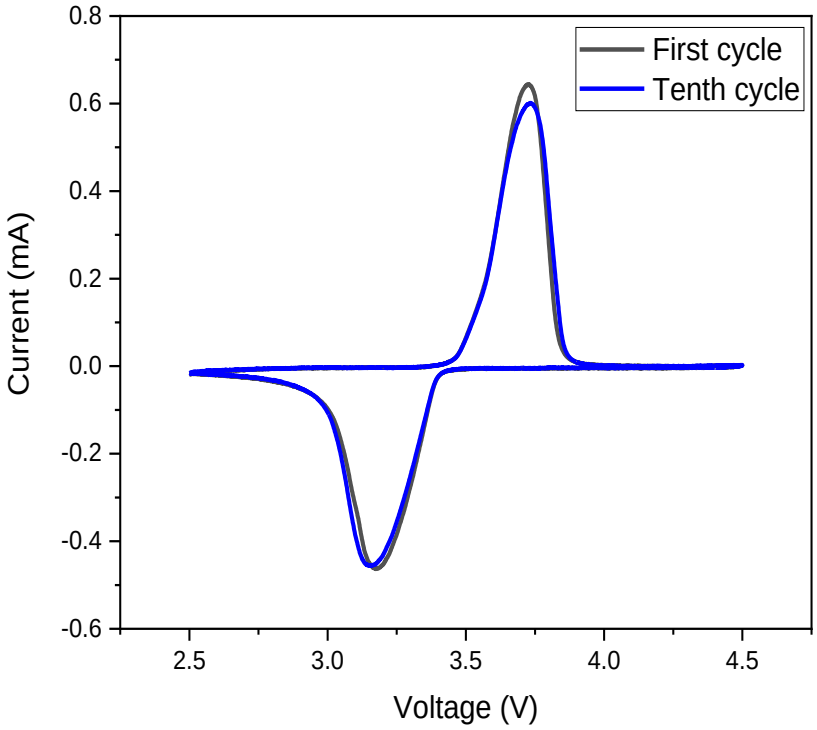

Figure 5.14. Cyclic voltammetry curves of $LiFePO_4$/C sample produced in way 3 first and tenth cycles at 0.1 mV/s.

In addition, the CV was obtained at various scan rates, as shown in Figure 5.15. Table 5.1. displays the anodic and cathodic peaks at various scan speeds. As the scan rates rise, the cathodic peak changes into the lower cell potential, while the anodic peak shifts towards the higher cell potential, increasing the potential difference between the redox peaks. This suggests that the polarization would be higher with higher charge discharge rates, and conversely.

Table 5.1. The cathodic and anodic peaks, as well as the potential difference.

Scan rate (mV/S)	Cathodic peak	Anodic peak	Potential difference
0.02	3.26	3.59	0.33
0.05	3.21	3.67	0.46
0.075	3.16	3.72	0.56
0.1	3.11	3.76	0.65
0.2	2.99	3.89	0.89

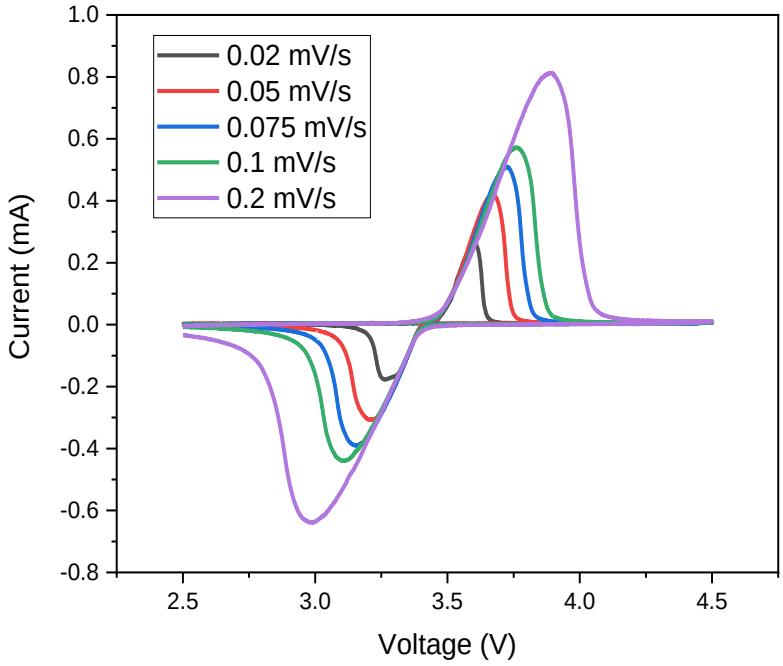

Figure 5.15. Cyclic voltammetry curves of $LiFePO_4$/C sample at various scan rates (from inner to outer: 0.02, 0.05, 0.075, 0.1, 0.2 mV/s).

5.2.4. Raman spectroscopic analysis

The Raman spectra of $LiFePO_4$ and $LiFePO_4$/C composites are shown in Figure 5.16. The symmetric $(PO4)^{3-}$ stretching mode of LFP is shown by a band at 950 cm^{-1} in all of the spectra. All of the curves have two distinct peaks at 1380 and 1570 cm-1, which correspond to the D and G carbon bands. The D and G bands in pure LFP are derived from leftover carbon from combustion synthesis. The G band develops in faulty graphene and graphite owing to planer vibrations of carbon atoms in the crystalline graphitic material and reflects the sp^2 carbon domains, whereas the D band appears

due to disordered vibrations of carbon atoms (sp^3 defects). The D band is missing or extremely weak in flawless graphite, and it is only active in the presence of defects and a reduction in the size of the in plane sp^2 domain. Furthermore, the ratio of these two bands measures the amount of flaws in carbonaceous material, with a lower ID/IG value indicating a higher graphitizing degree of the carbons. The measured ID/IG ratios for LFP and LFP/C composites are 1.382 and 0.907, respectively.

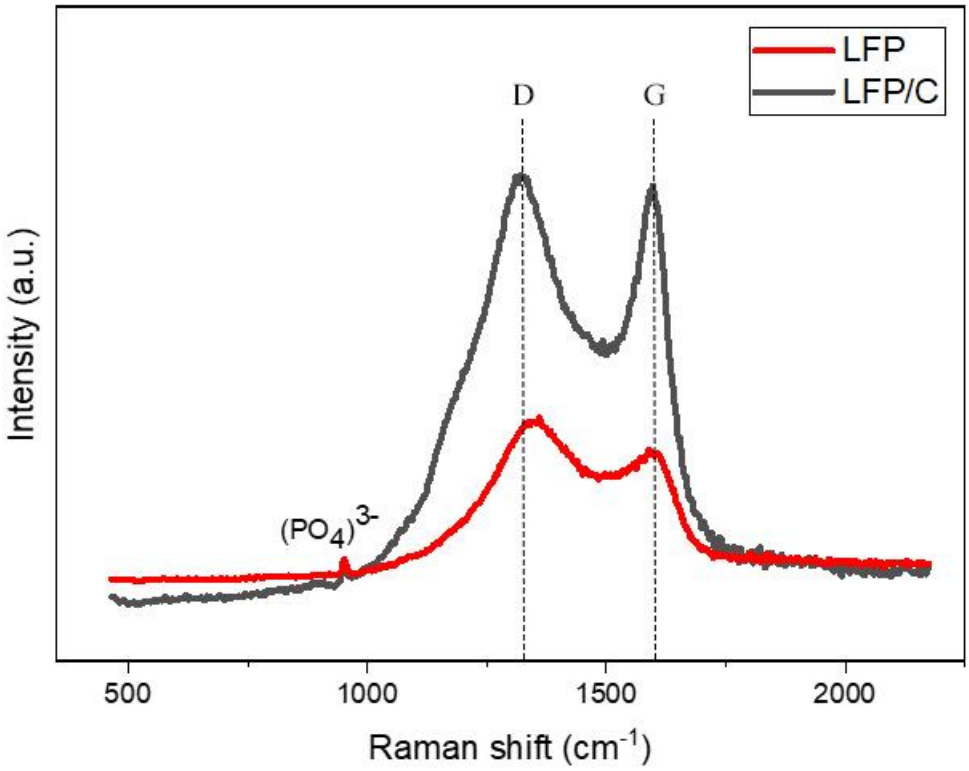

Figure 5.16. Raman spectra of $LiFePO_4$ and LFP/C composite.

5.3. Graphene Supported on a Carbon Coated $LiFePO_4$

The capacity of $LiFePO_4$/C which is 157 mAh/g still does not meet the theoretical capacity of $LiFePO_4$ which is 170 mAh/g and this is due to the fact that some lithium ions are unable to be entirely removed from the ordered-olivine structure, as a result of which capacity is lost. To explain why, two fundamental limiting factors have been identified: (i) Lithium ion phase-boundary diffusion is restricted due to the one-dimensional channels in LFP, which allow ionic disorder, foreign phases, and stacking defects to disrupt Li^+ transport. The mobility of a $LiFePO_4/FePO_4$ phase boundary is

impeded when Li^+ diffusion is disrupted, preventing parts of the cathode from accessing a reversible Li intercalation (Franger *et al.*, 2002). (ii) Low electron conductivity: the charges must be balanced throughout the charging and discharging processes due to the insertion/extraction of Li^+ via electron transfer. Electron movement will restrict Li^+ insertion/extraction and induce deterioration in electrochemical properties if electrons cannot travel quickly enough. Several efforts have been undertaken to enlarge the olivine structure's one-dimensional channels in order to enhance Li^+ transport and ease these difficulties. The properties of rGO make it an excellent choice for solving these issues.

5.3.1. Structural analysis of GO and rGO

The XRD profiles of GO and rGO are shown in Figure (5.17.). The graphene oxide diffraction peak at 2θ=11.0º at reflection plane (001) confirmed the formation of graphene oxide. After the thermal treatment, the reduction of GO was confirmed by diffraction peak that appeared at 2θ=26.8º, reflection plane (002) (Huang *et al.*, 2016). As shown in the diffractogram, the peak of GO disappeared, confirming the reduction of GO into rGO (Liu *et al.*, 2015).

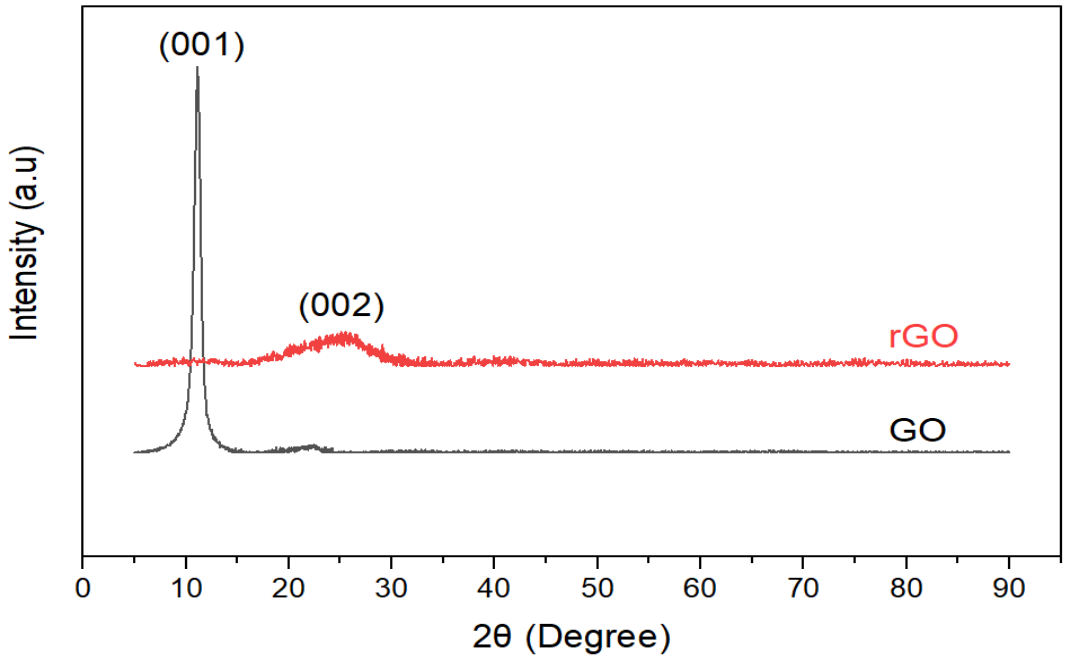

Figure 5.17. XRD patterns of graphene oxide (GO) and reduced graphene oxide (rGO).

5.3.2. Morphology

FESEM micrographs of GO made using a modified Hummers technique are shown in Figure 5.18.(a&b), indicating that the GO has a two-dimensional sheet-like structure. The FESEM pictures clearly show that GO has many lamellar layer structures, and the boundaries of each sheets can be recognized. The films are placed on top of one another and have wrinkled sections. The thickness of the GO sheets differed at the edges as well. because oxygen-containing functional groups were mostly joined at the GO's margins The GO sheets were securely suspended and did not bend, as seen by FESEM photos. According to the EDS analysis in Figure 5.18.(c), the GO comprises approximately 72.21 at. percent C and 27.79 at. percent O.

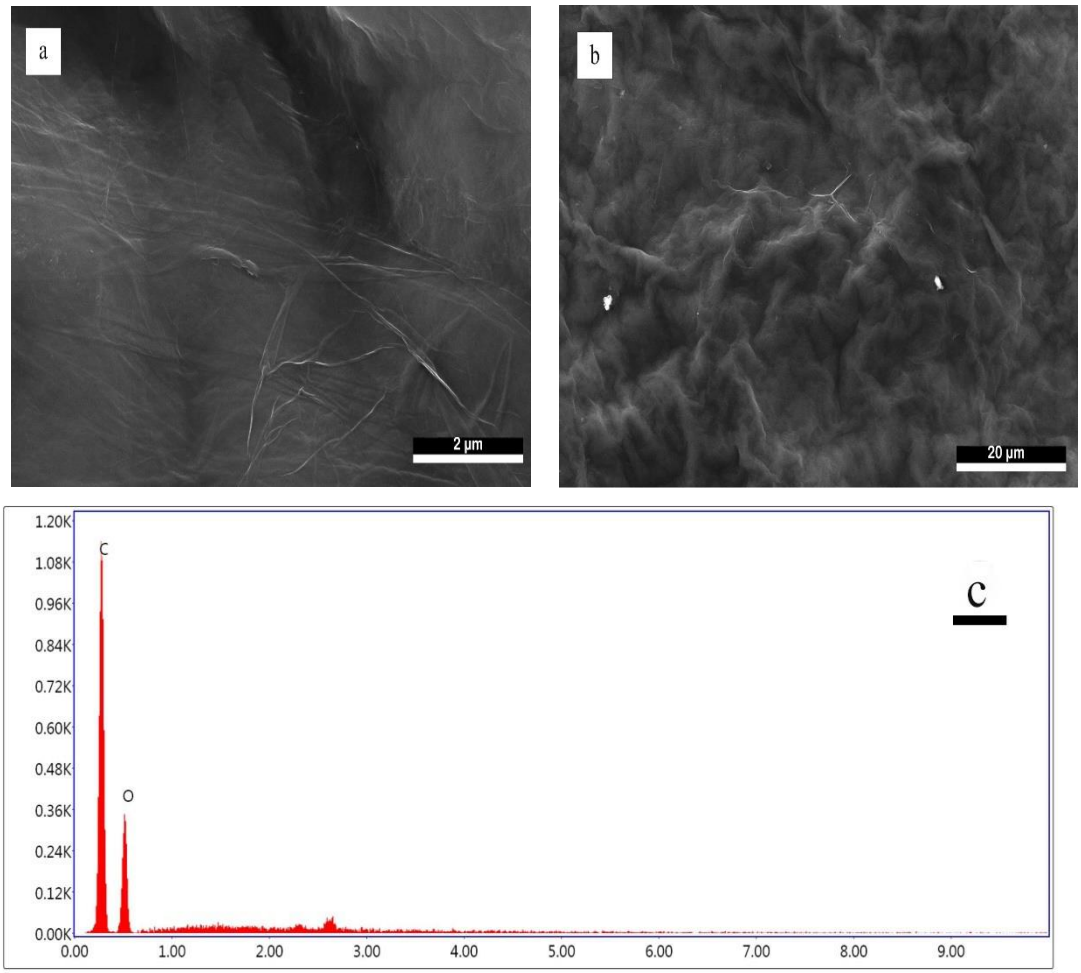

Figure 5.18.(a,b) FESEM of GO and Figure (c) EDS of GO.

The FESEM pictures of rGO gained from GO by the thermal reduction of GO. Figure 19.(a) & Figure 19.(b) shows the morphology of multilayer graphene. As can be seen in the Figure 5.19. , graphene layers have a wrinkled and transparent structure. The EDS analysis (Figure 19.(c)) indicates that the rGO sheets contain about 99.43 at.% C and 0.57 at.% O.

Figure 5.20 shows FESEM images of LFP/rGO with different amount of rGO (2-4%). RGO sheets in Figure 5.19. exhibit a curled morphology, with thin, wrinkled 'paper-like' structures. Additionally, The LFP nanoparticles were equally dispersed on the surface of rGO, according to FESEM (as with the FP particles).

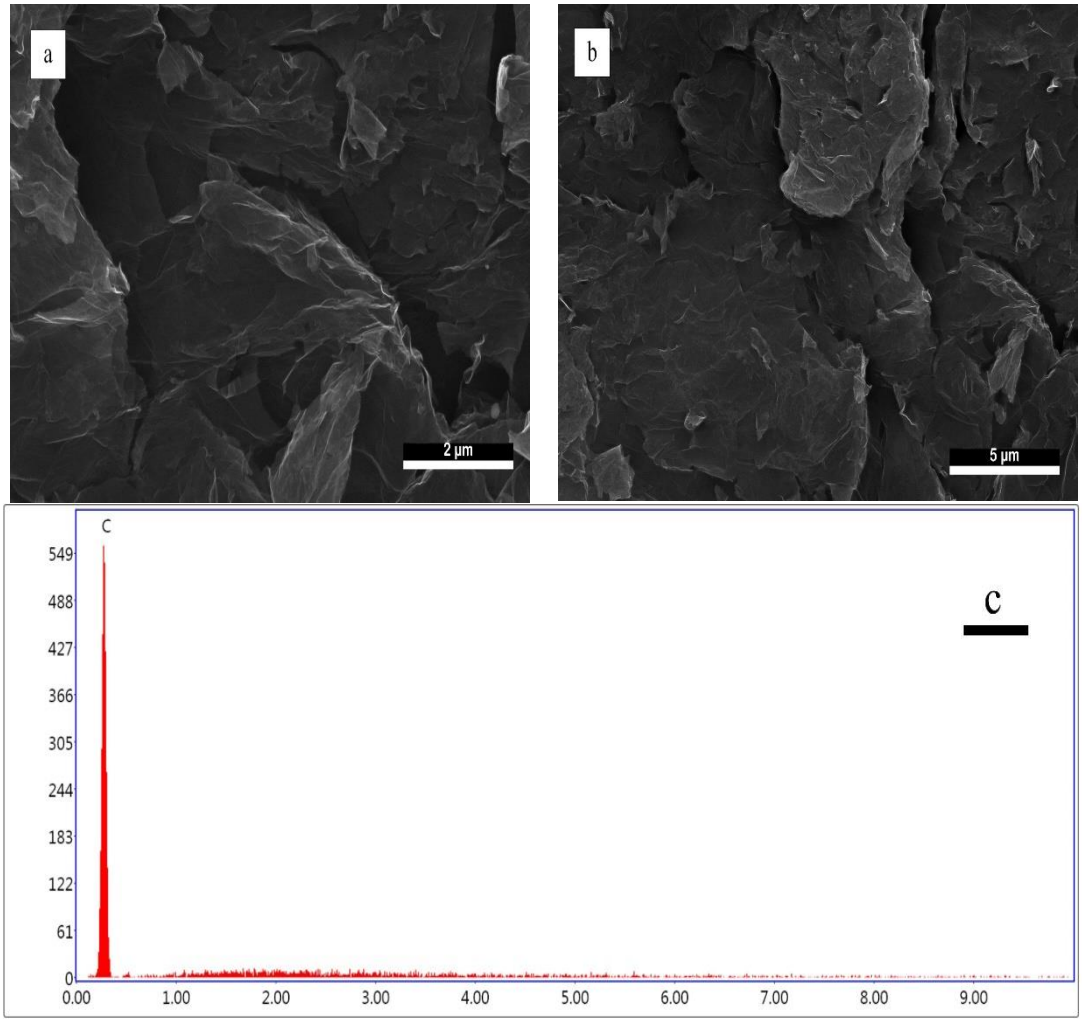

Figure 5.19. (a,b) FESEM of rGO and Figure (c) EDS of rGO.

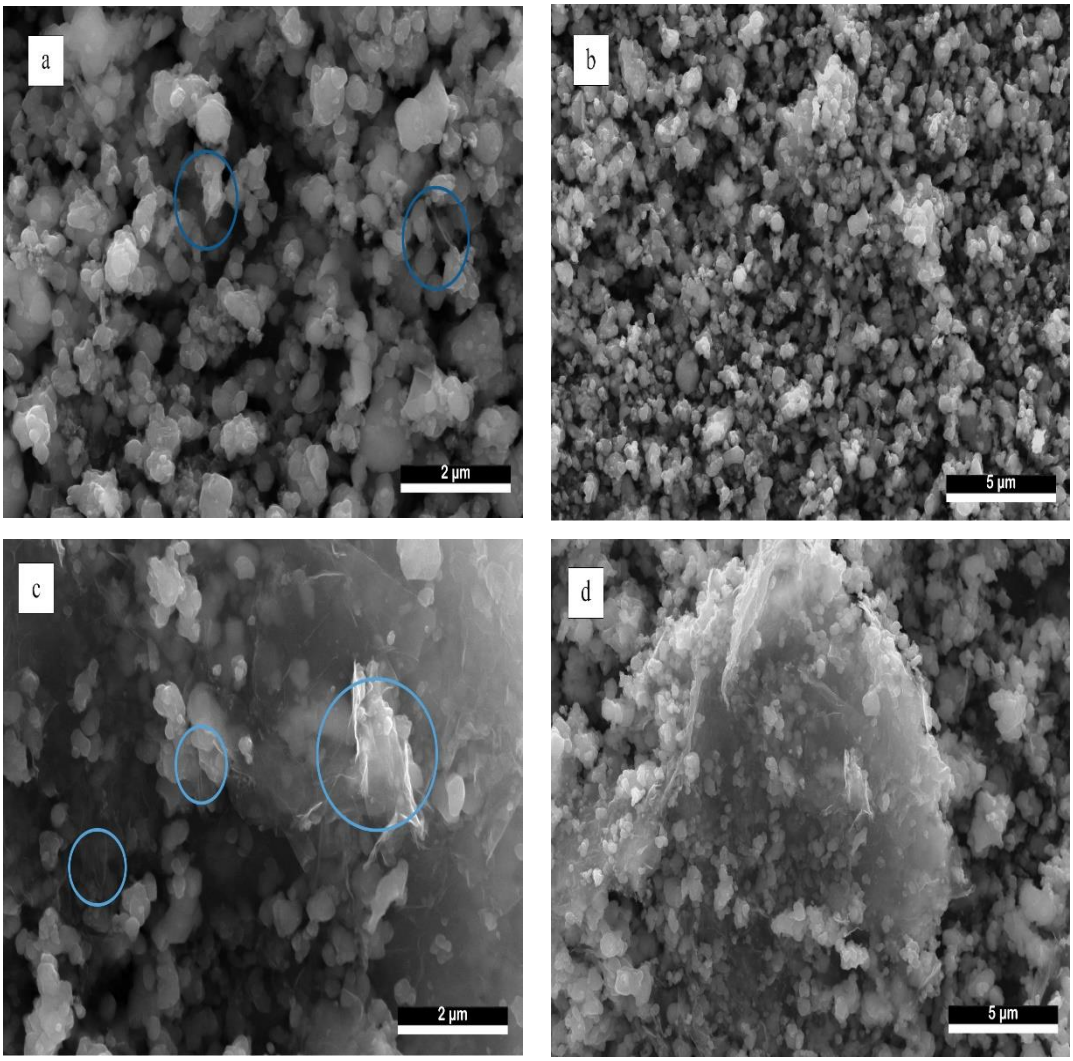

Figure 5.20. FESEM images of (a,b) LFP with a content of 2 wt% rGO , (c,d) LFP with a content of 4 wt% rGO.

Figure 5.21. shows the energy dispersive scanning spectroscopy (EDS) mapping images and EDS pattern of LFP/rGO with a content of 4% rGO, confirming that LFP and graphene were successfully combined. The EDS analysis of LFP/rGO sample suggests that the LFP/rGO sample contain about 7% C.

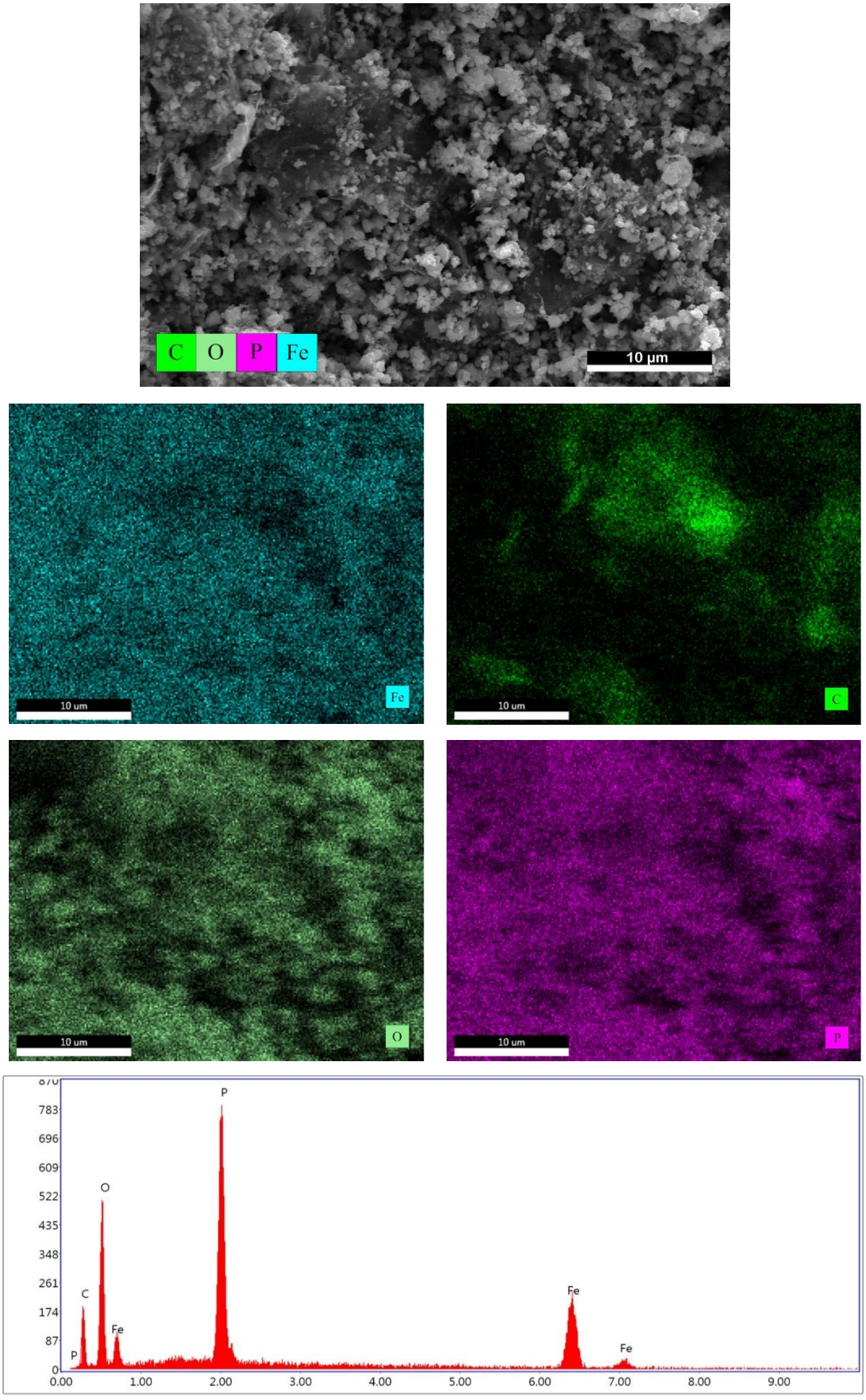

Figure 5.21. EDS mapping images and EDS spectrum of LFP/rGO with a content of 4% rGO.

5.3.3. Electrochemical performance of cLFP.rGO

The cLFP/rGO cathodes deliver the capacity from 175 to 197 mAh/g, based on the weight ratio of rGO (2 - 4 wt%) as shown in Figure 5.22. This is higher than the previously reported value of 120-160 mAh/g for synthesized cLFP. Interestingly, the measured values are higher than the theoretical capacity of 170 mAh/g theoretical capacity for LFP. The fact that the specific capacity rises with rGO concentration implies that rGO nanosheets are involved in Li^+ ion storage in the cLFP/rGO and that the storage process is reversible.

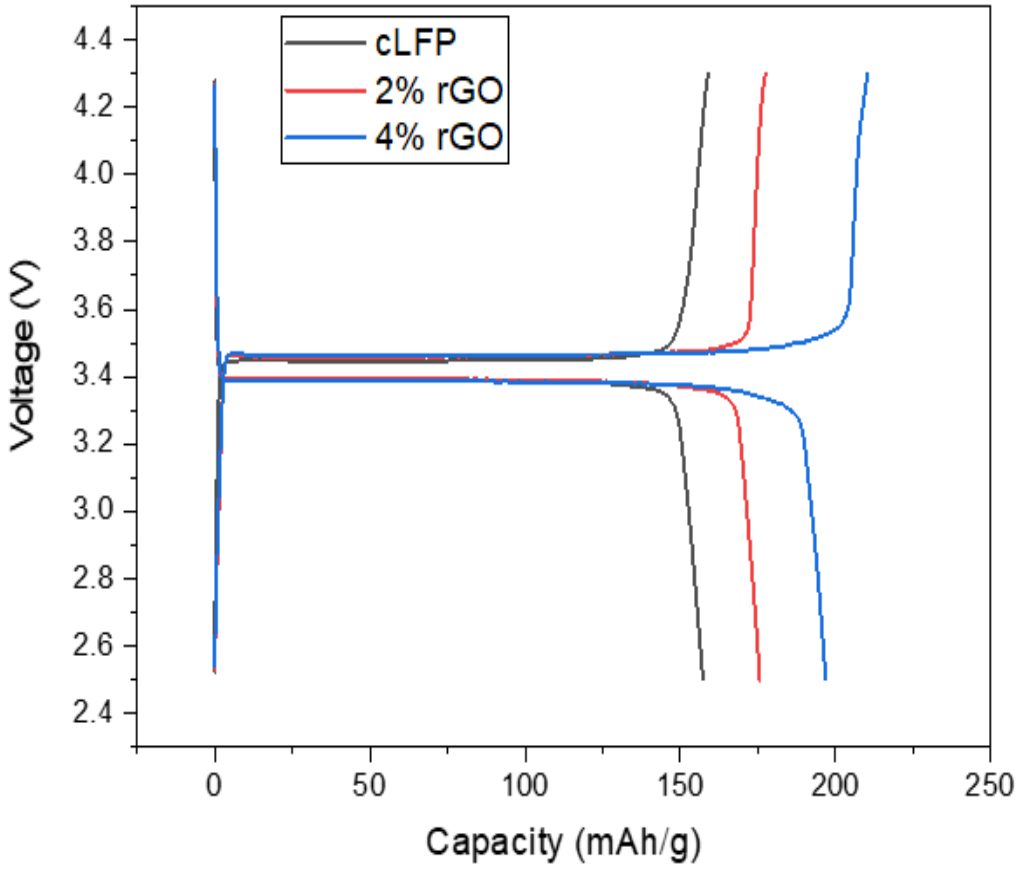

Figure 5.22. The first cycle of charging and discharging voltage profiles (at 0.1 C) of the carbon-coated LiFePO4 containing varying amounts of graphene (2 - 4 wt%).

The long-term charging and discharging of cLFP/rGO with 4% rGO has been performed (as shown in Figure 5.23.). After 100 cycles at 1C, the composites still provide a specific capacity of 170 mAh/g, thus showing 91% retention of initial

discharge capacity of 187 mAh/g while it was only 82% regard to cLFP and and the retention value for commercial LFP powder is 85%, whereas the retention value for bare LFP is higher (96%), indicating that this powder has few impurities. rGO resulted in a considerable increase in the electrochemical performance of LFP during charging and discharging, as a result of which outstanding cycling behavior was achieved. Two main factors are responsible for this improvement. One explanation is that it is feasible to input or remove lithium ions from both sides of rGO nanosheets. Another factor to consider is that during charging and discharging, the highly conductive rGO nanosheets that anchor the LFP particles function as rapid transport routes for electrons and lithium ions, improving the kinetics and reversibility of the lithium insertion-extraction cycles. Furthermore, the shape of rGO-wrapped LFP particles may contribute to increased rate performance, since electron transport on the LFP's surface may be rapid enough to tolerate high discharge/charge rates. The rGO also acts as a medium for the transfer of Li^+ ions across the boundaries of $LiFePO_4$ and $FePO_4$, allowing Li^+ ions to move swiftly during charging and discharging.

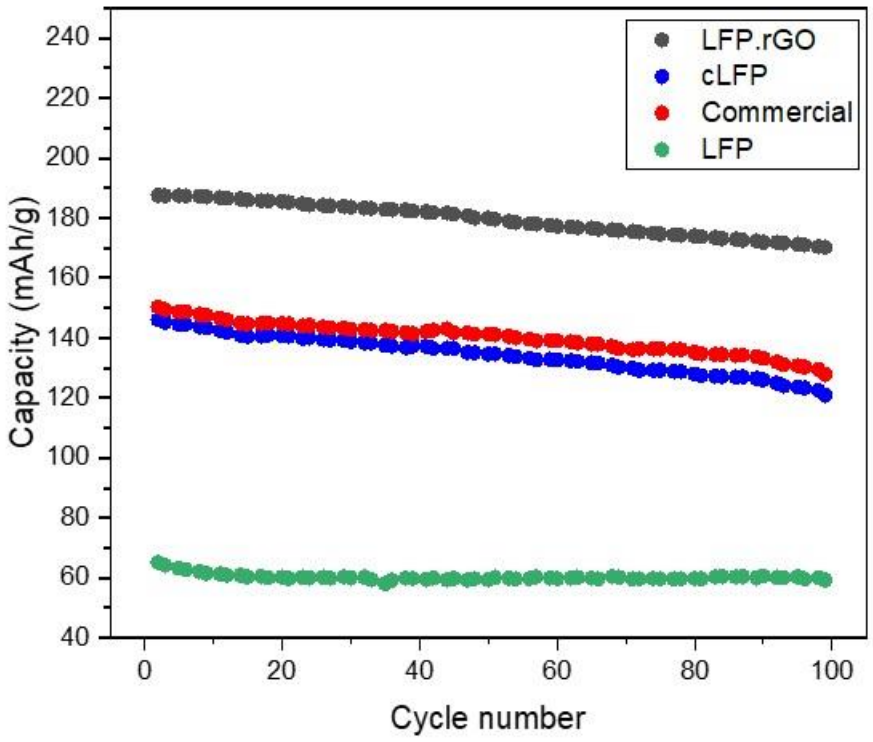

Figure 5.23. Cycling performance of bare LFP,commercial LFP, cLFP and cLFP.rGO(4% rGO) at 1C.

Figure 5.24. shows the discharge rate capability at various current densities of lithium ion battery cells with cathodes enhanced with 4wt% of graphene. For comparison, the graphene-free cLFP rate performance is also displayed. In line with expectations, with increased discharge rates, the capacity deteriorates very quickly due to the high discharging current that cannot be sustained (rapid Li^+ intercalation). Nevertheless, When operating at lower rates, 0.1-1C, cLFP.rGO delivers 24% more capacity; when operating at higher rates, 3-15C, it delivers 27% more capacity, clearly demonstrating the advantages of graphene. More specifically, the composite cathode material, cLFP.rGO, can provide a capacity of 131 mAh/g at a high discharging rate of 10 C, which is approximately 26% higher than the 98 mAh/g result from cLFP alone. For a range of C-rates, the coulombic efficiency of cLFP.rGO remains between 98 and 100 %.

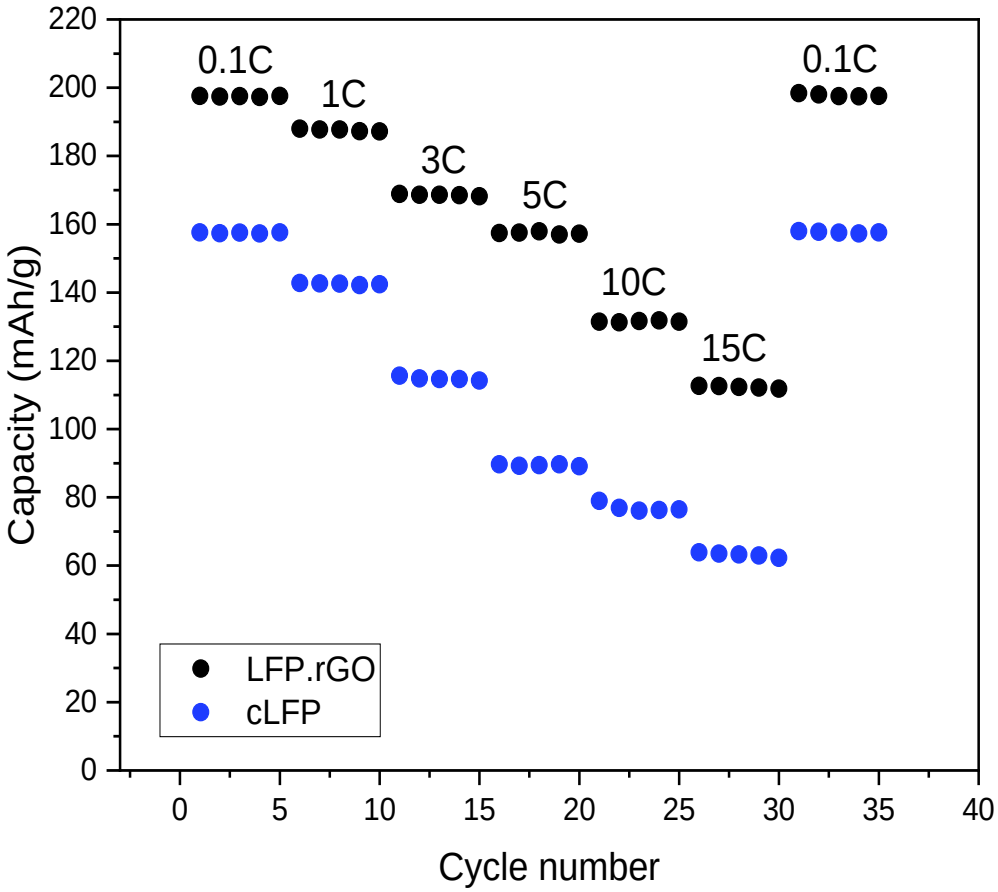

Figure 5.24. Rate performance of $LiFePO_4$ with 4wt% rGO at varying densities.

Figure 5.25. This graph depicts the cLFP/rGO cyclic voltammetry curve at a scanning rate of 0.1 mV/s. The LFP displays a pair of redox peaks in the anodic and cathodic directions, related to the extraction and insertion of lithium ions, at 3.82 V and 3.03 V, respectively. This reveals the mechanism of a single-electron reaction. The shapes of its oxidation peak and reduction peak barely changed after 5 cycles. This suggests that the material has good cyclic reversibility.

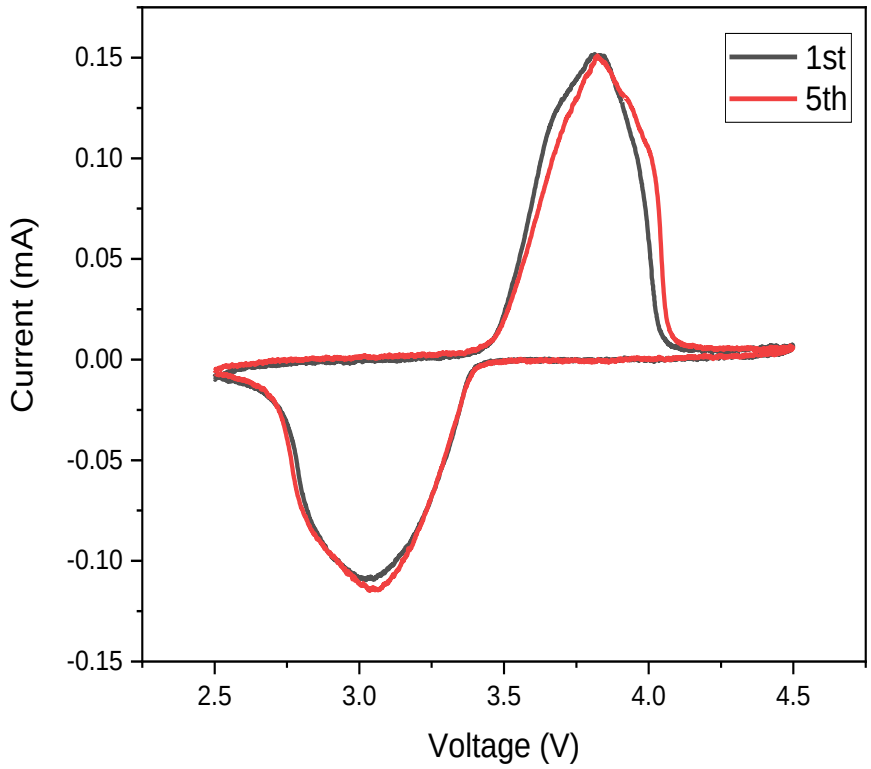

Figure 5.25. Cyclic voltammetry curves of LFP.rGO sample at 0.1 mV/s .

Electrochemical impedance spectroscopy was used to analyze the effect of rGO on internal resistance. The results are presented as Nyquist plots. Figure 5.26. shows the Nyquist plots for commercial LFP, 2LFP.rGO, and 4LFP.rGO. It is found that charge transfer resistance (R_2) decreases with increasing rGO. Li-ion diffusion is represented by a constant slope at low frequency owing to Warburg impedance (W_2). There is a higher diffusion of Li-ion with 4LFP.rGO than with LFP and 2LFP.rGO, as this line slopes upward.

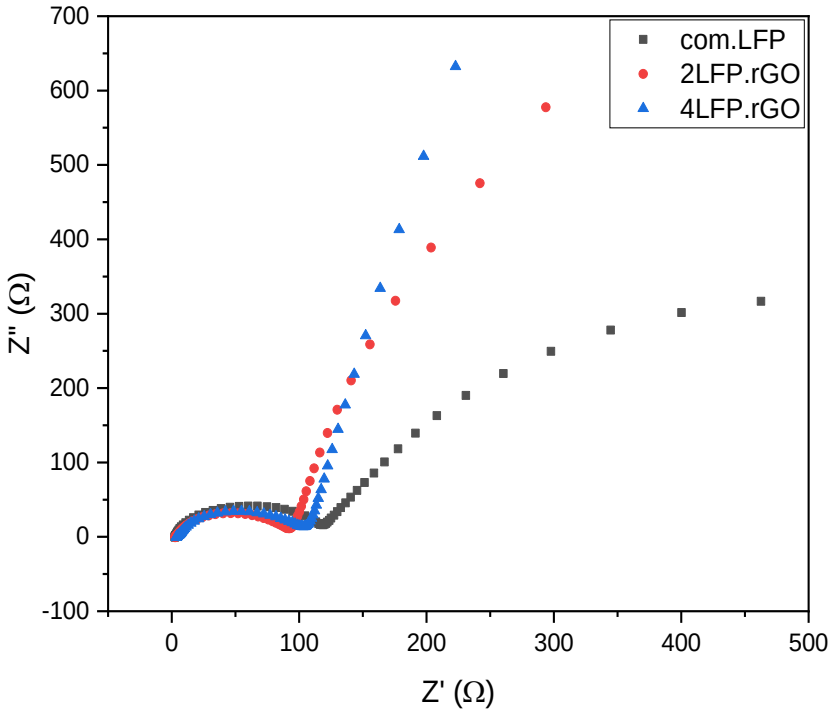

Figure 5.26. EIS of the commercial LiFePO4, 2LFP.rGO, 4LFP.rGO electrodes.

CHAPTER 6. CONCLUSION

In this study, $LiFePO_4$ material can be synthesized through the energy-efficient solution combustion process from a cheap trivalent iron compound. Different quantities of glycine fuel were used. The ratio of fuel to oxidant will determine flame temperatures and the composition of the surrounding atmosphere, which may affect the formation of $LiFePO_4$ phases. Carbon residuals and the degree of graphitization of carbon increased as the ratio of fuel to oxidant in the r reactant molecules increased. The increase in carbon content was always accompanied by a decrease in discharge capacity due to the formation of Fe_2P. Despite this, a sample synthesized by combustion synthesis with a 4:1 glycine to $LiFePO_4$ ratio had only 102 mAh/g greatest capacity of discharge at a 0.1 C rate.

Sucrose is a highly effective organic carbon source for enhancing $LiFePO_4$'s surface conductivity. Variable methods for introducing the organic carbon source resulted in different powder morphologies and carbon structures, which could lead to differences in the electrochemical performance of the $LiFePO_4$/C composites as-synthesized.Through adjusting the quantity of glycine and the manner of the addition of sucrose, the as-synthesized $LiFePO_4$/C sample demonstrated a high discharge capacity of 157 mAh/g at 0.1 C and outstanding rate performance at a high current density.

To further increase the capacity of carbon coating $LiFePO_4$ the graphene sheets were used to surround the $LiFePO_4$/C that had been produced. The addition of a little amount of graphene (2–4 wt.%) in $LiFePO_4$/C allows it to provide a discharge capacity of 175, 197 mAh/g, respectively, exceeding the theoretical capacity of 170 mAh/g of $LiFePO_4$ without causing obvious voltage polarization. A reversible redox interaction between the electrolyte's lithium ions and the graphene flakes is primarily responsible for the

increased capacity. The great redox potential of graphene flakes suggests that it could apply to other cathode materials for Li ion batteries as well.

REFERENCES

Nagaura .T, T. . (1990) 'No TitleLithium ion rechargeable battery, in: Batteries Solar Cells', p. 209.

Abe, H. *et al.* (2016) 'High-capacity thick cathode with a porous aluminum current collector for lithium secondary batteries', *Journal of Power Sources*, 334. doi: 10.1016/j.jpowsour.2016.10.016.

Allen, J. L., Richard Jow, T. and Wolfenstine, J. (2007) 'Kinetic study of the electrochemical FePO4 to LiFePO4 phase transition', *Chemistry of Materials*, 19(8). doi: 10.1021/cm062963o.

Andersson, A. S. *et al.* (2000) 'Thermal stability of LiFePO4-based cathodes', *Electrochemical and Solid-State Letters*, 3(2). doi: 10.1149/1.1390960.

Andersson, A. S. and Thomas, J. O. (2001) 'The source of first-cycle capacity loss in LiFePO4', *Journal of Power Sources*, 97(98). doi: 10.1016/S0378-7753(01)00633-4.

Armand, M. and Tarascon, J. M. (2008) 'Building better batteries', *Nature*. doi: 10.1038/451652a.

Arumugam, D., Paruthimal Kalaignan, G. and Manisankar, P. (2009) 'Synthesis and electrochemical characterizations of nano-crystalline LiFePO 4 and Mg-doped LiFePO 4 cathode materials for rechargeable lithium-ion batteries', *Journal of Solid State Electrochemistry*, 13(2). doi: 10.1007/s10008-008-0533-3.

Aruna, S. T., Muthuraman, M. and Patil, K. C. (1997) 'Combustion synthesis and properties of strontium substituted lanthanum manganites La1-xSrxMnO3 ($0 \leq x \leq 0.3$)', *Journal of Materials Chemistry*, 7(12). doi: 10.1039/a703901h.

Balakrishnan, P. G., Ramesh, R. and Prem Kumar, T. (2006) 'Safety mechanisms in lithium-ion batteries', *Journal of Power Sources*. doi: 10.1016/j.jpowsour.2005.12.002.

Belharouak, I., Johnson, C. and Amine, K. (2005) 'Synthesis and electrochemical analysis of vapor-deposited carbon-coated LiFePO4', *Electrochemistry Communications*, 7(10). doi: 10.1016/j.elecom.2005.06.019.

Cha, H. *et al.* (2018) 'Issues and Challenges Facing Flexible Lithium-Ion Batteries for Practical Application', *Small*. doi: 10.1002/smll.201702989.

Chabot, V. *et al.* (2014) 'A review of graphene and graphene oxide sponge: Material synthesis and applications to energy and the environment', *Energy and Environmental Science*. doi: 10.1039/c3ee43385d.

Chen, J. *et al.* (2008) 'The hydrothermal synthesis and characterization of olivines and related compounds for electrochemical applications', *Solid State Ionics*, 178(31–32). doi: 10.1016/j.ssi.2007.10.015.

Chen, L. *et al.* (2006) 'Binder effect on cycling performance of silicon/carbon composite anodes for lithium ion batteries', *Journal of Applied Electrochemistry*, 36(10). doi: 10.1007/s10800-006-9191-2.

Chen, Z. *et al.* (2004) 'Design of amorphous alloy electrodes for Li-ion batteries a big challenge', *Electrochemical and Solid-State Letters*, 7(10). doi: 10.1149/1.1792262.

Chen, Z., Christensen, L. and Dahn, J. R. (2003) 'Large-volume-change electrodes for Li-ion batteries of amorphous alloy particles held by elastomeric tethers', *Electrochemistry Communications*, 5(11). doi: 10.1016/j.elecom.2003.08.017.

Cheng, L. *et al.* (2010) 'General synthesis of carbon-coated nanostructure Li4 Ti 5O12 as a high rate electrode material for Li-ion intercalation', *Journal of Materials Chemistry*, 20(3). doi: 10.1039/b914604k.

Chernova, N. A. *et al.* (2009) 'Layered vanadium and molybdenum oxides: Batteries and electrochromics', *Journal of Materials Chemistry*, 19(17). doi: 10.1039/b819629j.

Chick, L. A. *et al.* (1990) 'Glycine-nitrate combustion synthesis of oxide ceramic powders', *Materials Letters*, 10(1–2). doi: 10.1016/0167-577X(90)90003-5.

Delmas, C. *et al.* (2008) 'Lithium deintercalation in LiFePO4 nanoparticles via a domino-cascade model', *Nature Materials*, 7(8). doi: 10.1038/nmat2230.

Devaraju, M. K. and Honma, I. (2012) 'Hydrothermal and solvothermal process towards development of LiMPO 4 (M = Fe, Mn) nanomaterials for lithium-ion batteries', *Advanced Energy Materials*. doi: 10.1002/aenm.201100642.

Ding, Y. *et al.* (2010) 'Preparation of nano-structured LiFePO4/graphene composites by co-precipitation method', *Electrochemistry Communications*, 12(1). doi: 10.1016/j.elecom.2009.10.023.

Doeff, M. M. *et al.* (2006) 'Optimization of carbon coatings on LiFePO4', *Journal of Power Sources*, 163(1 SPEC. ISS.). doi: 10.1016/j.jpowsour.2005.11.075.

Doeff, M. M. *et al.* (2008) 'Impact of carbon structure and morphology on the electrochemical performance of LiFePO 4/C composites', in *Journal of Solid State Electrochemistry*. doi: 10.1007/s10008-007-0419-9.

Dominko, R. *et al.* (2005) 'Impact of the Carbon Coating Thickness on the Electrochemical Performance of LiFePO[sub 4]/C Composites', *Journal of The Electrochemical Society*, 152(3). doi: 10.1149/1.1860492.

'Electrochimica Acta' (2004) *Electrochimica Acta*.

Ellis, B. *et al.* (2007) 'Synthesis of nanocrystals and morphology control of hydrothermally prepared LiFePO4', *Journal of Materials Chemistry*, 17(30). doi: 10.1039/b705443m.

Ferg, E. *et al.* (1994) 'Spinel Anodes for Lithium-Ion Batteries', *Journal of The Electrochemical Society*, 141(11). doi: 10.1149/1.2059324.

Ferrari, S. *et al.* (2010) 'Influence of particle size and crystal orientation on the electrochemical behavior of carbon-coated LiFePO4', *Journal of Physical Chemistry C*, 114(29). doi: 10.1021/jp1025834.

Franger, S. *et al.* (2002) 'LiFePO4 synthesis routes for enhanced electrochemical performance', *Electrochemical and Solid-State Letters*, 5(10). doi: 10.1149/1.1506962.

Gaberscek, M., Dominko, R. and Jamnik, J. (2007) 'Is small particle size more important than carbon coating? An example study on LiFePO4 cathodes', *Electrochemistry Communications*, 9(12). doi: 10.1016/j.elecom.2007.09.020.

Gallagher, K. G. *et al.* (2016) 'Optimizing Areal Capacities through Understanding the Limitations of Lithium-Ion Electrodes', *Journal of The Electrochemical Society*, 163(2). doi: 10.1149/2.0321602jes.

Geim, A. K. and Novoselov, K. S. (2007) 'The rise of graphene', *Nature Materials*, 6(3). doi: 10.1038/nmat1849.

Golubkov, A. W. *et al.* (2014) 'Thermal-runaway experiments on consumer Li-ion batteries with metal-oxide and olivin-type cathodes', *RSC Advances*, 4(7). doi: 10.1039/c3ra45748f.

Gong, Z. and Yang, Y. (2011) 'Recent advances in the research of polyanion-type cathode materials for Li-ion batteries', *Energy and Environmental Science*. doi: 10.1039/c0ee00713g.

Ha, H., Shanmuganathan, K. and Ellison, C. J. (2015) 'Mechanically stable thermally crosslinked poly(acrylic acid)/reduced graphene oxide aerogels', *ACS Applied Materials and Interfaces*, 7(11). doi: 10.1021/acsami.5b00407.

Herle, P. S. *et al.* (2004) 'Nano-network electronic conduction in iron and nickel olivine phosphates', *Nature Materials*, 3(3). doi: 10.1038/nmat1063.

Hochgatterer, N. S. *et al.* (2008) 'Silicon/graphite composite electrodes for high-capacity anodes: Influence of binder chemistry on cycling stability', *Electrochemical and Solid-State Letters*, 11(5). doi: 10.1149/1.2888173.

Hu, Y. *et al.* (2004) 'Electrochemical Performance of Sol-Gel Synthesized LiFePO[sub 4] in Lithium Batteries', *Journal of The Electrochemical Society*, 151(8). doi: 10.1149/1.1768546.

Huang, H., Yin, S. C. and Nazar, L. F. (2001) 'Approaching theoretical capacity of LiFePO4 at room temperature at high rates', *Electrochemical and Solid-State Letters*, 4(10). doi: 10.1149/1.1396695.

Huang, X. *et al.* (2016) 'Tunable electromagnetic properties and enhanced microwave absorption ability of flaky graphite/cobalt zinc ferrite composites', *Journal of Alloys and Compounds*, 662. doi: 10.1016/j.jallcom.2015.12.076.

Hummers, W. S. and Offeman, R. E. (1958) 'Preparation of Graphitic Oxide', *Journal of the American Chemical Society*, 80(6). doi: 10.1021/ja01539a017.

Jugović, D. and Uskoković, D. (2009) 'A review of recent developments in the synthesis procedures of lithium iron phosphate powders', *Journal of Power Sources*. doi: 10.1016/j.jpowsour.2009.01.074.

Julien, C. *et al.* (2000) 'Combustion synthesis and characterization of substituted lithium cobalt oxides in lithium batteries', *Solid State Ionics*, 135(1–4). doi: 10.1016/S0167-2738(00)00370-2.

Julien, C. M. *et al.* (2014) 'Comparative issues of cathode materials for Li-ion batteries', *Inorganics*, 2(1). doi: 10.3390/inorganics2010132.

Kang, W. *et al.* (2012) 'Ethylene glycol-assisted nanocrystallization of LiFePO 4 for a rechargeable lithium-ion battery cathode', *CrystEngComm*, 14(6). doi: 10.1039/c2ce06423e.

Kim, J. K. *et al.* (2008) 'Enhancement of electrochemical performance of lithium iron phosphate by controlled sol-gel synthesis', *Electrochimica Acta*, 53(28). doi: 10.1016/j.electacta.2008.06.049.

Kim, Keun Soo *et al.* (2009) 'Large-scale pattern growth of graphene films for stretchable transparent electrodes', *Nature*, 457(7230). doi: 10.1038/nature07719.

Laffont, L. *et al.* (2006) 'Study of the LiFePO4/FePO4two-phase system by high-resolution electron energy loss spectroscopy', *Chemistry of Materials*, 18(23). doi: 10.1021/cm0617182.

Larry Feinberg (2016) 'Quantity surveyors go "Green"', *Engineering News*, 2017(Dec / Jan 2017).

Lestriez, B. *et al.* (2007) 'On the binding mechanism of CMC in Si negative electrodes for Li-ion batteries', *Electrochemistry Communications*, 9(12). doi: 10.1016/j.elecom.2007.10.001.

Liang, G. *et al.* (2008) 'Lithium iron phosphate with high-rate capability synthesized through hydrothermal reaction in glucose solution', in *Journal of Power Sources*. doi: 10.1016/j.jpowsour.2008.02.056.

Liu, G. *et al.* (2015) 'A reduced graphene oxide modified metallic cobalt composite with superior electrochemical performance for supercapacitors', *RSC Advances*, 5(78). doi: 10.1039/c5ra09748g.

Liu, H. *et al.* (2006) 'Kinetic study on LiFePO4/C nanocomposites synthesized by solid state technique', *Journal of Power Sources*, 159(1 SPEC. ISS.). doi: 10.1016/j.jpowsour.2005.10.098.

Liu, J. *et al.* (2009) 'Long-term cyclability of LiFePO4/carbon composite cathode material for lithium-ion battery applications', *Electrochimica Acta*, 54(24). doi: 10.1016/j.electacta.2009.05.003.

Liu, W. R. *et al.* (2005) 'Enhanced cycle life of Si anode for Li-ion batteries by using modified elastomeric binder', *Electrochemical and Solid-State Letters*, 8(2). doi: 10.1149/1.1847685.

M.S. Whittingham (2004) *Chemical Reviews*.

Morgan, D., Van der Ven, A. and Ceder, G. (2004) 'Li Conductivity in LixMPO4 (M = Mn, Fe, Co, Ni) Olivine Materials', *Electrochemical and Solid-State Letters*, 7(2). doi: 10.1149/1.1633511.

Nanjundaswamy, K. S. *et al.* (1996) 'Synthesis, redox potential evaluation and electrochemical characteristics of NASICON-related-3D framework compounds', *Solid State Ionics*, 92(1–2). doi: 10.1016/s0167-2738(96)00472-9.

Nitta, N. *et al.* (2015) 'Li-ion battery materials: Present and future', *Materials Today*. doi: 10.1016/j.mattod.2014.10.040.

Nitta, N. and Yushin, G. (2014) 'High-capacity anode materials for lithium-ion batteries: Choice of elements and structures for active particles', *Particle and Particle Systems Characterization*. doi: 10.1002/ppsc.201300231.

Noh, M. *et al.* (2005) 'Amorphous carbon-coated tin anode material for lithium secondary battery', *Chemistry of Materials*, 17(8). doi: 10.1021/cm0481372.

Oh, S. M. *et al.* (2010) 'The effects of calcination temperature on the electrochemical performance of LiMnPO4 prepared by ultrasonic spray pyrolysis', *Journal of Alloys and Compounds*, 506(1). doi: 10.1016/j.jallcom.2010.07.010.

Ou, X. Q. *et al.* (2008) 'LiFePO4 doped with magnesium prepared by hydrothermal reaction in glucose solution', *Chinese Chemical Letters*, 19(3). doi: 10.1016/j.cclet.2007.10.052.

Padhi, A. K. *et al.* (1997) 'Effect of Structure on the Fe3 + / Fe2 + Redox Couple in Iron Phosphates', *Journal of The Electrochemical Society*, 144(5). doi: 10.1149/1.1837649.

Padhi, A. K. and Goodenough, J. B. (1997) *Phospho-olivine as positive electrodes materials for rechargeable lithium batteries* , *J. Electroanal. Chem*.

Padhi, A. K., Nanjundaswamy, K. S. and Goodenough, J. B. (1997) 'Phospho-olivines as Positive-Electrode Materials for Rechargeable Lithium Batteries', *Journal of The Electrochemical Society*, 144(4). doi: 10.1149/1.1837571.

Palacín, M. R. (2009) 'Recent advances in rechargeable battery materials: A chemist's perspective', *Chemical Society Reviews*, 38(9). doi: 10.1039/b820555h.

Du Pasquier, A. *et al.* (2003) 'A comparative study of Li-ion battery, supercapacitor and nonaqueous asymmetric hybrid devices for automotive applications', *Journal of Power Sources*, 115(1). doi: 10.1016/S0378-7753(02)00718-8.

Raja, M. W. *et al.* (2009) 'Synthesis of nanocrystalline Li4Ti5O12 by a novel aqueous combustion technique', *Journal of Alloys and Compounds*, 468(1–2). doi: 10.1016/j.jallcom.2007.12.072.

Rao, B. M. L., Francis, R. W. and Christopher, H. A. (1977) 'Lithium-Aluminum Electrode', *Journal of The Electrochemical Society*, 124(10). doi: 10.1149/1.2133098.

Ravet, N. *et al.* (2001) 'Electroactivity of natural and synthetic triphylite', in *Journal of Power Sources*. doi: 10.1016/S0378-7753(01)00727-3.

Saravanan, K. *et al.* (2010) 'Morphology controlled synthesis of LiFePO4/C nanoplates for Li-ion batteries', *Energy and Environmental Science*, 3(4). doi: 10.1039/b923576k.

Song, H. K. *et al.* (2010) 'Recent progress in nanostructured cathode materials for lithium secondary batteries', *Advanced Functional Materials*, 20(22). doi: 10.1002/adfm.201000231.

Song, Q. *et al.* (2011) 'Effect of pH value on particle morphology and electrochemical properties of LiFePO4 by hydrothermal method', *Materials Research Bulletin*, 46(9). doi: 10.1016/j.materresbull.2011.05.015.

Spong, A. D., Vitins, G. and Owen, J. R. (2006) 'A Solution—Precursor Synthesis of Carbon-Coated LiFePO4 for Li-Ion Cells.', *ChemInform*, 37(11). doi: 10.1002/chin.200611012.

Su, F. Y. *et al.* (2010) 'Flexible and planar graphene conductive additives for lithium-ion batteries', *Journal of Materials Chemistry*, 20(43). doi: 10.1039/c0jm01633k.

Takahashi, M. *et al.* (2001) 'Characterization of LiFePO4 as the cathode material for rechargeable lithium batteries', in *Journal of Power Sources*. doi: 10.1016/S0378-7753(01)00728-5.

Takahashi, M. *et al.* (2002) 'Reaction behavior of LiFePO4 as a cathode material for rechargeable lithium batteries', in *Solid State Ionics*. doi: 10.1016/S0167-2738(02)00064-4.

Tarascon, J. M. and Armand, M. (2001) 'Issues and challenges facing rechargeable lithium batteries', *Nature*. doi: 10.1038/35104644.

Thackeray, M. (2002) 'An unexpected conductor', *Nature Materials*, 1(2). doi: 10.1038/nmat736.

Wang, G. *et al.* (2010) 'Mesoporous LiFePO4/C nanocomposite cathode materials for high power lithium ion batteries with superior performance', *Advanced Materials*, 22(44). doi: 10.1002/adma.201002045.

Wang, G., Shen, X. and Yao, J. (2009) 'One-dimensional nanostructures as electrode materials for lithium-ion batteries with improved electrochemical performance', *Journal of Power Sources*, 189(1). doi: 10.1016/j.jpowsour.2008.10.044.

Wang, J. S. *et al.* (2011) 'Formulation and characterization of ultra-thick electrodes for high energy lithium-ion batteries employing tailored metal foams', *Journal of Power Sources*, 196(20). doi: 10.1016/j.jpowsour.2011.06.071.

Wang, L. *et al.* (2010) 'A facile method of preparing mixed conducting LiFePO4/graphene composites for lithium-ion batteries', *Solid State Ionics*, 181(37–38). doi: 10.1016/j.ssi.2010.09.056.

Wang, Y. and Cao, G. (2008) 'Developments in nanostructured cathode materials for high-performance lithium-ion batteries', *Advanced Materials*. doi: 10.1002/adma.200702242.

Wang, Y., He, P. and Zhou, H. (2011) 'Olivine LiFePO4: Development and future', *Energy and Environmental Science*. doi: 10.1039/c0ee00176g.

Whittingham, M. S. *et al.* (2005) 'Some transition metal (oxy)phosphates and vanadium oxides for lithium batteries', *Journal of Materials Chemistry*, 15(33). doi: 10.1039/b501961c.

Whittingham, M. S. (2008) 'Materials challenges facing electrical energy storage', *MRS Bulletin*, 33(4). doi: 10.1557/mrs2008.82.

Winter, M. and Besenhard, J. O. (1999) 'Electrochemical lithiation of tin and tin-based intermetallics and composites', *Electrochimica Acta*, 45(1). doi: 10.1016/S0013-4686(99)00191-7.

Wood, D. L., Li, J. and Daniel, C. (2015) 'Prospects for reducing the processing cost of lithium ion batteries', *Journal of Power Sources*, 275. doi: 10.1016/j.jpowsour.2014.11.019.

Xia, Y., Yoshio, M. and Noguchi, H. (2006) 'Improved electrochemical performance of LiFePO4 by increasing its specific surface area', *Electrochimica Acta*, 52(1). doi: 10.1016/j.electacta.2006.05.002.

Xiao, H. *et al.* (2017) 'Reduced-Graphene Oxide/Poly(acrylic acid) Aerogels as a Three-Dimensional Replacement for Metal-Foil Current Collectors in Lithium-Ion Batteries', *ACS Applied Materials and Interfaces*, 9(27). doi: 10.1021/acsami.7b07283.

Yamada, A. *et al.* (2003) 'Olivine-type cathodes: Achievements and problems', in *Journal of Power Sources*. doi: 10.1016/S0378-7753(03)00239-8.

Yamada, A., Chung, S. C. and Hinokuma, K. (2001) 'Optimized LiFePO[sub 4] for Lithium Battery Cathodes', *Journal of The Electrochemical Society*, 148(3). doi: 10.1149/1.1348257.

Yang, J. *et al.* (2011) 'Electrochemical performances of Co-doped LiFePO4/C obtained by hydrothermal method', *Journal of Alloys and Compounds*, 509(37). doi: 10.1016/j.jallcom.2011.07.021.

Yang, S., Zavalij, P. Y. and Whittingham, M. S. (2001) 'Hydrothermal synthesis of lithium iron phosphate cathodes', *Electrochemistry Communications*, 3(9). doi: 10.1016/S1388-2481(01)00200-4.

Yang, W. *et al.* (1999) 'A combustion method to prepare spinel phase LiMn2O4 cathode materials for lithium-ion batteries', *Journal of Power Sources*, 81–82. doi: 10.1016/S0378-7753(99)00219-0.

Yazami, R. and Touzain, P. (1983) 'A reversible graphite-lithium negative electrode for electrochemical generators', *Journal of Power Sources*, 9(3). doi: 10.1016/0378-7753(83)87040-2.

Yuan, L. X. *et al.* (2011) 'Development and challenges of LiFePO4 cathode material for lithium-ion batteries', *Energy and Environmental Science*. doi: 10.1039/c0ee00029a.

Zaghib, K. *et al.* (2008) 'Surface effects on the physical and electrochemical properties of thin $LiFePO_4$ particles', *Chemistry of Materials*, 20(2). doi: 10.1021/cm7027993.

Zhang, W.-J. (2010) 'Comparison of the Rate Capacities of LiFePO[sub 4] Cathode Materials', *Journal of The Electrochemical Society*, 157(10). doi: 10.1149/1.3460840.

Zhang, W. M. *et al.* (2008) 'Carbon coated Fe3O4 nanospindles as a superior anode material for lithium-ion batteries', *Advanced Functional Materials*, 18(24). doi: 10.1002/adfm.200801386.

Zhao, H. *et al.* (2008) 'Electrochemical characterization of micro-sized Sb/SnSb composite anode', *Materials Chemistry and Physics*, 110(2–3). doi: 10.1016/j.matchemphys.2008.02.002.

Zhou, X. *et al.* (2011) 'Graphene modified LiFePO4 cathode materials for high power lithium ion batteries', *Journal of Materials Chemistry*, 21(10). doi: 10.1039/c0jm03287e.

RESUME

Name Surname **:** Ali Jamal Abdulkareem

EDUCATION

Degree	School	Graduation Year
Master's	Sakarya University / Natural Science Institute / Nanoscience and Nanoengineering	Continuing
Undergraduate	Mustansiriyah University / Faculty Of Engineering / Department Of Materials Engineering	2016
High School	Al-Markaziya High School	2012

WORK EXPERIENCE

Year	Place	Position
2020-Present	Sakarya University	Researcher

FOREIGN LANGUAGES

Arabic	Native level
English	Advanced level
Turkish	Lower intermediate level

HOBBIES

Reading, Learning languages, Sports, Traveling